Changing ENSO in a warming climate

Wenju Cai[*,1,2,3], Agus Santoso[3,4,5], Matthew Collins[6], Boris Dewitte[7,8,9], Christina Karamperidou[10], Jong-Seong Kug[11], Matthieu Lengaigne[12], Michael J. McPhaden[13], Malte F. Stuecker[14], Andréa S.Taschetto[4,5], Axel Timmermann[15,16], Lixin Wu[1,2], Sang-Wook Yeh[17], Guojian Wang[1,2,3], Benjamin Ng[3], Fan Jia[19], Yun Yang[19], Jun Ying[20,21], Xiao-Tong Zheng[1,2], Tobias Bayr[22], Josephine R. Brown[23], Antonietta Capotondi[24,25], Kim M. Cobb[26], Bolan Gan[1,2], Tao Geng[1], Yoo-Geun Ham[27], Fei-Fei Jin[10], Hyun-Su Jo[27], Xichen Li[28,29], Xiaopei Lin[1,2], Shayne McGregor[30], Jae-Heung Park[11], Karl Stein[15,16], Kai Yang[31], Li Zhang[1,2], and Wenxiu Zhong[21,32]

1. Frontier Science Centre for Deep Ocean Multispheres and Earth System and Physical Oceanography Laboratory, Ocean University of China, Qingdao, China.
2. Qingdao National Laboratory for Marine Science and Technology, Qingdao, China.
3. Centre for Southern Hemisphere Oceans Research (CSHOR), CSIRO Oceans and Atmosphere, Hobart 7004, Australia.
4. Climate Change Research Centre, University of New South Wales, Sydney, Australia
5. ARC Centre of Excellence for Climate Extremes, University of New South Wales, Australia
6. College of Engineering Mathematics and Physical Sciences, University of Exeter, Laver Building, North Park Road, Exeter, EX4 4QE, UK.
7. Centro de Estudios Avanzado en Zonas Áridas (CEAZA), La Serena, Chile.
8. Departamento de Biología, Facultad de Ciencias del Mar, Universidad Católica del Norte, Coquimbo, Chile.
9. Millennium Nucleus for Ecology and Sustainable Management of Oceanic Islands (ESMOI), Coquimbo, Chile.
10. Department of Atmospheric Sciences, University of Hawai'i at Mānoa, Hawaii, USA.
11. Division of Environmental Science & Engineering, Pohang University of Science and Technology (POSTECH), Pohang, South Korea.
12. MARBEC, Université Montpellier, CNRS, Ifremer, IRD, Sète, France.
13. NOAA/Pacific Marine Environmental Laboratory, Seattle, Washington 98115, USA.
14. Department of Oceanography and International Pacific Research Center, School of Ocean and Earth Science and Technology, University of Hawai'i at Mānoa, Honolulu, HI, USA.
15. Center for Climate Physics, Institute for Basic Science (IBS), Busan, South Korea.
16. Pusan National University, Busan, South Korea.
17. Department of Marine Sciences and Convergent Technology, Hanyang University, ERICA, Ansan, South Korea.
18. CAS Key Laboratory of Ocean Circulation and Waves, Institute of Oceanology/Center for Ocean Mega - Science, Chinese Academy of Sciences, 7 Nanhai Road, Qingdao 266071, China.
19. College of Global Change and Earth System Science, Beijing Normal University, Beijing, China.
20. State Key Laboratory of Satellite Ocean Environment Dynamics, Second Institute of Oceanography, Ministry of Natural Resources, Hangzhou, 310012, China.
21. Southern Marine Science and Engineering Guangdong Laboratory (Zhuhai), Zhuhai, China.
22. GEOMAR Helmholtz Centre for Ocean Research Kiel, Kiel, Germany.
23. School of Earth Sciences, University of Melbourne, Parkville, VIC, Australia.
24. NOAA/Physical Sciences Laboratory, Boulder, CO, USA.
25. Cooperative Institute for Research in Environmental Sciences, University of Colorado, Boulder, Colorado, USA.
26. School of Earth & Atmospheric Sciences, Georgia Institute of Technology, 311 Ferst Drive, Atlanta, USA.
27. Department of Oceanography, Chonnam National University, Gwangju, South Korea
28. Institute of Atmospheric Physics, Chinese Academy of Sciences, Beijing, China.
29. University of Chinese Academy of Sciences, Beijing, China.
30. School of Earth, Atmosphere and Environment, Monash University, Clayton, Victoria, Australia.
31. State Key Laboratory of Numerical Modeling for Atmospheric Sciences and Geophysical Fluid Dynamics, Institute of Atmospheric Physics, Chinese Academy of Sciences, Beijing, China.
32. School of Atmospheric Sciences, and Guangdong Province Key Laboratory for Climate Change and Natural Disaster Studies, Sun Yat-sen University, Guangzhou, China

*Corresponding author: wenju.cai@csiro.au

Abstract | Originating in the equatorial Pacific, El Niño-Southern Oscillation (ENSO) has highly consequential global impacts. ENSO's response to greenhouse warming is therefore one of the most important issues of climate science today. There is an inter-model consensus of an increase in future ENSO rainfall variability, but debate continues on the disparity between observed and projected tropical Pacific mean state change, and its ramifications for projected ENSO change. Progress has been made on the response of ENSO sea surface temperature (SST) variability, the role of internal variability, and the effects of remote ocean forcing in the ENSO response. In this review, we synthesise these advances. Models that best capture key ENSO dynamics tend to project an increase in future ENSO SST variability and an eastward shift and intensification of ENSO teleconnections under greenhouse warming, consistent with paleoclimate evidence of stronger ENSO variability since the 1950s compared to past centuries. The increase in ENSO variability, though underpinned by increased equatorial Pacific upper ocean stratification, is strongly influenced by internal ENSO variability, raising issues about its quantifiability and detectability. Ongoing coordinated community efforts and computational advances are enabling long-simulation, large-ensemble experiments, and high-resolution modelling, offering encouraging prospects for alleviating model biases, incorporating fundamental dynamical processes, and reducing uncertainties in projections.

Key Points

- Under greenhouse warming, majority of climate models project a faster background warming in the eastern equatorial Pacific with an increase in ENSO rainfall variability. This SST warming pattern continues for a century after global mean temperature stabilises.

- ENSO rainfall response in the equatorial Pacific intensifies and shifts eastward, leading to an eastward intensification of extratropical teleconnections.

- The observed equatorial Pacific surface warming pattern since 1980, though opposite to the projected faster warming in the equatorial eastern Pacific, is within the inter-model range in terms of SST gradients and is subject to influence from internal variability.

- Variability of ENSO SST and extreme ENSO events are projected to increase under greenhouse warming, with a stronger inter-model consensus in the latest generation of climate models, but time of emergence for ENSO SST variability is later than that for ENSO rainfall variability, opposite to that for mean SST versus mean rainfall.

- The future ENSO change is likely influenced by past variability, such that quantification of future ENSO in the only realization of the real world is challenging.

- Although there is no definitive relationship of ENSO variability with the mean zonal SST gradient or seasonal cycle, paleoclimate records suggest a causal connection between vertical temperature stratification and ENSO strength, and a greater ENSO strength since the 1950s than in past centuries, supporting an emerging increase in ENSO variability under greenhouse warming.

El Niño-Southern Oscillation (ENSO), an alternation between warm phase El Niño and cold phase La Niña events, is the most consequential year-to-year climate phenomenon on the planet[1,2,3]. During El Niño, as in the 2015-2016 extreme event[4,5], an anomalous warming in the central and eastern equatorial Pacific weakens the west-minus-east zonal sea surface temperature (SST) gradient along the equator. The associated weakening of the trade winds in turn intensifies the warm anomaly, a process referred to as Bjerknes feedback[6]. Atmospheric convection over the west Pacific moves eastward, resulting in global impacts that include droughts and forest fires in countries bordering the western Pacific, but torrential rains and floods in regions of the eastern equatorial Pacific[1,2,3,7,8]. During a La Niña event, anomalously low SST occurs in the central and eastern Pacific, convection over the western Pacific intensifies and becomes more concentrated, and global impacts roughly opposite to those of El Niño occur. ENSO's global reach affects agriculture, public health, infrastructure, transportation, water security, ecosystems, and biodiversity[1,2,3,9].

Because of its widespread and consequential impacts, how ENSO may change in a warming climate is one of the most compelling issues in climate change research today. A series of the Intergovernmental Panel on Climate Change (IPCC) assessments[10,11] have found that long-term climatic conditions have changed, with historically high anthropogenic emissions of greenhouse gases post 1990. Furthermore, there is no sign on the horizon that there will be an abatement of these emissions, highlighting the urgency to understand ENSO's response to greenhouse warming now and in the future[12,13].

Likely future ENSO changes and underpinning dynamics have been periodically synthesized[12,13] (**Fig. 1**). In a framework of ocean-atmosphere instability, in which ENSO is sensitive to ocean-atmosphere coupling between equatorial trade winds and the west-minus-east zonal SST gradient[1,14,15,16], a mean state change with weakened trade winds and a reduced west-minus-east zonal SST gradient, as projected by most climate models[12,13], would imply that ENSO would become more unstable[16], therefore favoring greater amplitude under global warming. However, from the 1990s, when climate models were first used to investigate ENSO response to greenhouse forcing[17,18], to the fifth IPCC assessment report[10], climate models had shown no consensus on ENSO SST variability change in conventionally defined regions in the central-eastern equatorial Pacific.

Instead, as synthesized in a 2015 review[13], models that more realistically simulate characteristics of extreme ENSO events tend to project systematic changes. These changes include an increased frequency of El Niño events with extreme rainfall in the eastern

equatorial Pacific[19-22], more frequent extreme equatorward swings of large-scale convergence zones[23], a higher frequency of El Niño events featuring eastward propagating SST anomalies[24], and a higher frequency of extreme La Niña events[25]. The projected changes are consistent with proxy records of ENSO variability suggesting that twentieth-century ENSO activity is stronger than that during the previous centuries[26,27,28]. A key development is a realization that projection of the fundamental variable of ENSO SST variability should be made at ENSO anomaly centres unique to each climate model[29]. Meanwhile, advances continue on our understanding of processes controlling the mean state changes[30-33], ENSO's interactions with variability in other ocean basins[34], and role of internal variability of the climate system in the response of ENSO SST variability[35-38]. Although uncertainty remains, an inter-model consensus on increased ENSO SST variability is emerging, with additional support from models participating in the sixth phase of Coupled Model Intercomparison Projects[39] (CMIP6).

In this review, we summarize the advances since 2015. We begin by describing ENSO event diversity and asymmetry, changing ENSO in observations and proxy-data, and mean state impacts on ENSO feedbacks. We subsequently discuss factors that contribute to the observed and projected mean state changes. We continue by outlining the projected ENSO SST variability change and associated mechanism, focusing on proposed mechanisms involving mean state changes and other factors such as internal variability and inter-basin interactions (**Fig. 1**). We then synthesize insight from paleo-proxy records in ENSO sensitivity to external forcing. The review ends with identification of uncertainties and prospects for improved quantification, detection, and high-resolution modelling of ENSO SST variability change.

ENSO in observations

An important advance in ENSO research is the discovery that ENSO events are diverse and their anomaly centres can be in the equatorial eastern Pacific (EP) or central Pacific (CP)[8,40-44]. Observed ENSO evolution and the associated feedbacks therefore need to be assessed in terms of the diversity, as summarised in this section.

ENSO event diversity and asymmetry

Strong El Niño events tend to peak in the EP, whereas strong La Niña and moderate El Niño events tend to peak in the CP region, and La Niña events tend to be weaker than EP El Niño events, and last for multiple years contributing to ENSO diversity and asymmetry[5,42-45] (**Fig. 2, a-d**). The EP ENSO and CP ENSO can be approximated by spatially-fixed indices of SST anomaly such as Niño3 (averaged SST anomaly over 5°S-5°N, 150°W-90°W) and Niño4 (5°S-5°N, 160°E-150°W), respectively, of which the combination is captured by the Niño3.4 (5°S-5°N, 170°W-120°W) index. The fundamental dynamics for ENSO diversity and asymmetry is a nonlinear Bjerknes feedback, whereby after anomalous warming in the eastern Pacific locally triggers atmospheric deep convection, zonal winds respond nonlinearly

with a greater response to additional warming. The nonlinear wind response leads to further warming, resulting in an extreme EP El Niño, a process distinctively weaker in the central Pacific[44,46]. Heat discharge of the equatorial Pacific during strong El Niño cools the equatorial Pacific subsurface conducive to development of La Niña. Mathematically, the dynamics is reflected by a nonlinear relationship between the leading two Empirical Orthogonal Functions of tropical Pacific SST variability such that their linear combination represents EP and CP ENSO events, referred to as E-index and C-index[29,46,47,48]. For observations, time series of Niño3 and Niño4 can be approximately represented by E-index and C-index (**Fig. 2a, b**)**,** respectively.

Observed ENSO changes

ENSO has been changing. At the turn of the 21st century, there was a marked increase in occurrences of CP El Niño events, which are weaker than EP El Niño events, contributing to weaker ENSO SST variability[49]. Since the 1970s, statistically significant changes have been shown to occur in the evolution of El Niño and La Niña events from their embryonic to fully mature stages[50], with both CP and EP ENSO events tending to originate from the western Pacific, rather than the central and eastern Pacific before the 1970s[51]. Since late 1950s, CP and EP ENSO variability has shown an increasing trend[52,53,54]. Using data further back in time, both EP-ENSO and CP-ENSO variability show an approximately 20% increase in the post-1960 compared to the pre-1960 period (**Fig. 2a, b**), characterised by more frequent extreme El Niño and extreme La Niña, respectively, with asymmetric spatial patterns (**Fig. 2c, d**) and impact. However, there is uncertainty in data before the 1950s due to sparse observations and sampling errors[55] which makes assessment of a potential impact of greenhouse warming difficult.

Multiple paleo-ENSO proxy datasets do point to an approximately 25% intensification of ENSO variability during the late 20th Century, relative to the pre-industrial period or before[26,27,28,56-59]. The intensification is supported by ENSO reconstructions that show greater CP[57,60] and EP[58] ENSO variability relative to the pre-industrial era. While these results imply that anthropogenic greenhouse forcing might have already contributed to an increase in ENSO variability, because these proxy records reflect both ENSO-related temperature and rainfall variability, the extent of an increase in SST variability is unclear.

ENSO feedbacks and mean state

Observations since 1950 have identified ocean-atmosphere feedbacks responsible for ENSO SST anomaly growth. During an El Niño, mean upwelling of cold water in the eastern equatorial Pacific and the mean subsurface horizonal advection act to strengthen the climatological horizontal and vertical SST gradients, and thus damp an initial warm SST anomaly. In addition to this mean advective damping, the warm SST anomaly promotes deep atmospheric convection and increasing tropical cloud amounts, consequently reducing surface radiative and latent and sensible heat fluxes into the ocean, a process referred to as thermal damping. On the other hand, the warm SST anomaly and the associated west-

minus-east SST gradient is reinforced by weakened equatorial trade winds through three positive feedbacks[12,61,62,63]: the Ekman feedback, in which the weakened trade winds reduce upwelling of mean cold subsurface water in the eastern equatorial Pacific; the thermocline feedback, whereby the weakened trade winds lead to a flattened thermocline with anomalously warm subsurface water that is advected by mean upwelling to the surface; and the zonal advective feedback, in which the weakened trade winds reduce the mean westward oceanic transport of cold waters from the eastern Pacific. The relative importance of the feedback processes differs across events. During a CP El Niño, for instance, the zonal advective feedback tends to be more important than the thermocline feedback. Nonetheless, the three positive feedbacks increase with the upper ocean stratification of the equatorial Pacific[29,64-67].

Thus, the background climate state of the equatorial Pacific Ocean affects ENSO feedbacks and ENSO intensity[1,14,15,16]. Therefore, assessing ENSO response to greenhouse warming requires an understanding of how the tropical Pacific mean state will change.

Changes in mean state

Based on ocean-atmosphere reanalyses[68,69,70], the observed mean state changes since 1980s, in which emissions of greenhouse gases increase substantially, feature a strong strengthening of the Walker circulation, west-minus-east SST gradient and equatorial easterly winds[71-74] (**Fig. 3a**). However, the simulated multi-model averaged changes by state-of-the-art climate models over the same period are small (**Fig. 3b**), and the projected future mean state changes are generally opposite to the observed since the 1980s (compare **Fig. 3a** and **Fig. 3c**). The climate models, while continuing to show a persistent too-cold and too-west equatorial Pacific cold-tongue bias (**Fig. 3d**), project a tropical Pacific future mean state change that features a weakening of the Walker Circulation, a reduction of the equatorial west-minus-east SST gradient, and an enhanced equatorial warming compared to off-equatorial regions[12,13,75] (**Fig. 3b**). Trends over the 1980-2019 period of the west-minus-east SST gradients in individual models and in the reanalyses show that the observed changes since the 1980s are within the inter-model range (**Fig. 3e**), before the long-term reductions in the west-minus-east SST gradients in majority of models emerge (**Fig. 3f**). In this section, we outline processes that contribute to the observed and projected future mean state changes, and their differences.

Forcing of the observed mean state changes since 1980

The observed changes result from a balance of several processes including atmospheric damping differential between the west and the east, an oceanic thermostat mechanism in the east, internal variability on multidecadal scales, and inter-basin interactions. Most of these processes contribute to the enhanced west-minus-east SST gradient.

West-east damping differential. The mean SST, and hence evaporative damping, is higher in the western Pacific than in the east[76,77,78]. In addition, the higher mean SST in the western Pacific induces a greater net negative cloud-radiation feedback compared to the east[79]. These two processes are conducive to a reduced equatorial west-minus-east zonal SST gradient[78], which in turn weakens equatorial easterly winds through Bjerknes feedback, leading to the enhanced equatorial warming strongest in the east[76,77].

Ocean thermostat. On the other hand, assuming that the ocean is in quasi-equilibrium with greenhouse gas forcing, these changes in atmospheric processes must be compensated by changes in oceanic processes. Consistently, ocean upwelling in the equatorial eastern Pacific can facilitate divergence of some of the added heat away from the eastern Pacific cold tongue region, favouring less warming in the eastern than the western Pacific-an ocean thermostat mechanism[80] also amplified by the Bjerknes feedback.

Internal variability. Multidecadal internal variability might also contribute to the observed enhancement in the zonal SST gradient since 1980. However, limitations of *in situ* observations and reanalyses have hindered an unambiguous attribution of the equatorial Pacific trends since the 1980s to either natural or anthropogenic causes[33,81]. For instance, satellite-observed changes indicate a smaller strengthening of the Walker Circulation than implied by reanalyses[33]. While the satellite trend is still opposite to the simulated changes averaged over large ensemble of model simulations, some ensemble members are also able to reproduce the observed strengthening of the Walker Circulation[33]and the equatorial zonal SST gradients[81] (**Fig. 3e**), despite an overall underestimation of internal decadal variability in models[82]. Thus, internal multi-decadal variability could be offsetting greenhouse warming-induced changes and therefor leading to the observed trend since 1980s[33,81,83], which is, therefore, likely transient in nature[81].

Inter-basin interactions. Interactions with the two other tropical oceans on multi-decadal timescales are shown to also play an important role in forcing the observed intensification of zonal SST gradient since 1980 (REF.[34]) (**Fig. 3a**). There has been faster warming in the tropical Indian Ocean[84], Atlantic[85,86], or both[87,88] since 1980, with anomalous atmospheric sinking motion in the tropical Pacific conducive to an enhanced equatorial easterly surface wind trend, and hence to a cooling in the eastern Pacific[85].

Processes affecting projected future mean state changes

For the projected long-term mean state changes, the competing processes between the atmospheric damping differential and the oceanic thermostat mechanism also operate, whereas multidecadal internal variability plays a diminishing role. Studies have found that state-of-the-art climate models underestimate inter-basin interactions[30,34,89,90,91], which might contribute to the long-term faster warming in the equatorial eastern Pacific than otherwise the case[34]. Additional factors that influence future mean state changes include impact from off-equatorial Pacific Ocean warming, ENSO rectification, and the too-cold and too-west

equatorial Pacific cold tongue bias in climate models, though their relative importance is unclear and likely model-dependent.

Off-equatorial Pacific warming. The equatorial Pacific mean state changes involve processes outside the equatorial Pacific. The equatorial warming can partly be forced by oceanic subduction of anomalous off-equatorial warming advected towards the equatorial upwelling region, or a weakening of the Hadley circulation and wind-driven oceanic subtropical overturning cells[92,93]. Because of the multidecadal timescale involved in the off-equatorial forcing, modelling studies suggest a mean state change with an initially strengthened zonal SST gradient from the oceanic thermostat mechanism followed decades later by a gradient weakening through oceanic subduction of anomalous off-equatorial warming[92,93,94]. This time-varying mean state change is supported by a modelling study showing that models and ensemble members in a signal model that simulate historical strengthening of the zonal SST gradient commonly exhibit a reversed future trend[81].

ENSO rectification. While mean state changes such as the equatorial SST warming pattern and enhanced stratification can change the balance of ENSO feedbacks and thereby ENSO variability[29,75,95], ENSO variability change can rectify onto the mean state altering the warming pattern in the tropical Pacific via nonlinear oceanic temperature advection[96,97]. For example, if extreme El Niño events become less frequent relative to La Niña events, a La Niña–like mean state warming can emerge[96], although this is a case seen in only a small number of models. In models with realistic nonlinear dynamical heating, that is, an anomalous oceanic advection of temperature anomalies, or in models with realistic nonlinear Bjerknes feedback, an increase in ENSO variability contributes to the emergence of an El Niño-like warming pattern[29,97].

Cold tongue bias. Common present-day model biases within the tropical Pacific are suggested to have contributed to a fast warming in the east in most climate models[30,31,32]. For example, the common too-cold and too-west cold tongue (**Fig. 3d**) might produce excessive SST sensitivity to radiative warming in the cold tongue region, resulting in the erroneous warming and weakening in west-minus-east SST gradient[32]. On the other hand, the cold tongue bias can lead to an overestimated ocean thermostat mechanism under greenhouse warming and spuriously weak shortwave radiation reduction in response to surface warming in the central-to-western Pacific[98] such that alleviation of this bias would favour a faster eastern Pacific warming than in the west[95]. Despite the disparity between the observed changes since 1980 and the projected future changes, the change might not be unidirectional but time-varying. For example, the change in mean west-minus-east SST gradient could initially be dominated by oceanic thermostat and subsequently by other processes leading to opposite trends in late 21st century[92,93,94].

In terms of changes in the upper ocean temperature structure, ocean reanalyses over the 1910-2017 period show an intensified equatorial Pacific upper-ocean stratification[51]. Although the extent to which the intensified stratification is due to internal variability or greenhouse warming is unclear, the increased stratification is consistent with the projected change for the

21st century when a transient increase in CO_2 continues[13]. The intensified stratification underpins the projected increase in ENSO SST variability over the 21st century, as summarised in the upcoming sections.

Projected ENSO variability changes

Climate model projections of ENSO SST change have generally been based on conventional ENSO SST indices evaluated at fixed anomaly centres defined from observations[12,13,35,99], such as Niño3, without considering ENSO diversity. Projected changes in SST variability at the fixed centre show no inter-model consensus. Much progress has occurred since the 90's in understanding ENSO response to greenhouse forcing (see timeline in **Fig. 1**), including that the lack of the inter-model consensus was in part due to competing changes between the main ENSO linear positive and negative feedbacks despite robust change in individual feedback term[12,63,100,101,102] (**Fig. 1**, by 2010).

Robust changes emerged in key characteristics that underpin ENSO extremes[19,21,24,25,75,103,104] (**Fig. 1,** by 2015); for example, a doubling in frequency of El Niño events with extreme rainfall impacts from about one event per 20 years in the century before 1990 to one event per 10 years in the century after[21]. Such increasing frequency is also seen in CMIP6 models[20,105], and continues for as long as a century even after global mean temperature stabilises at the warming target of the Paris Agreement, that is, 1.5-2.0°C warming relative to the pre-industrial level[22,106].

Subsequently (by 2018, **Fig. 1**), emerging projection of enhanced ENSO SST variability was found at anomaly centres unique to individual CMIP3 and CMIP5 models[29] in models with more realistic ENSO diversity and nonlinearity, which are underestimated by most models[29,107,108]. The increase in ENSO SST variability is supported by CMIP6 models[109] with a stronger inter-model consensus, as outlined below.

Increased ENSO SST variability

The locations of ENSO SST anomaly centres can be different across models and from those observed by as much as 30° longitude[29]. Therefore, assessment of ENSO SST variability change should consider CP and EP ENSO anomaly centres simulated in individual models, and recent increased model agreement is partially due to correcting for model-specific anomaly centres[29]. Climate models tend to simulate a weaker distinction between EP and CP events than observed[29]. However, in CMIP5 models that reasonably simulate the distinction between these two types of events, EP ENSO variance is projected to increase by approximately 15% from the century before 2000 to the century after 2000 under 'business as usual' emission scenario, with 88% of models producing an increase; CP ENSO variance is also projected to increase, although the inter-model agreement is low[29] (59%). Similar conclusions were found in an analysis of 11 CMIP6 models[109]. A larger group of 23 CMIP6 models show an even stronger inter-model agreement, with all 23 models (100%) which

capture EP and CP events, generating an enhanced EP ENSO variance (**Fig. 4a**) and 65% of the models generating an increase in CP ENSO variance (**Fig. 4b**). The stronger inter-model agreement may be related to modest improvements in the simulated ENSO, such as pattern and event diversity, and a slight reduction in the Pacific mean state biases[110,111]. An overall increase in climate sensitivity[112] might also be a factor. Even without model selection, the majority of CMIP6 models generate an increase in Niño3 and Niño4 SST variability, with 28 and 27 out of 34 models, respectively, producing an increase of about 10-15% when comparing variability over the 20th and 21st centuries.

The enhanced variability in EP and CP ENSO is associated with more occurrences of extreme EP El Niño and extreme La Niña events[29] (**Fig. 4c, d**), increasing from 5.6 and 5.6 events per century in the present-day to 8.9 and 8.3 events per century in the future climate, respectively. In particular, dramatic swings from an extreme EP El Niño in a year to an extreme La Niña the next year (**Fig. 4c, d**), as seen in 1997-1998, increase from 1.1 events per century in the present day to 2.8 events per century in the future climate.

The implication of increased ENSO SST variability is expected to be greater than the changes in teleconnection *per se* would suggest, due to the compounding effect of the mean state change. In the presence of faster warming in the eastern equatorial Pacific Ocean than in the surrounding regions, even weak El Niño events are able to induce strong atmospheric convection[13,21,64,104]. This would lead to extreme impacts via atmospheric teleconnection as discussed next.

Eastward intensification of teleconnections

As a result of a projected faster warming in eastern equatorial Pacific under greenhouse warming, the mean convection center shifts eastward during during both CP and EP ENSO events[113-119], and the response of tropical eastern Pacific rainfall to ENSO strengthens[19,20,21] (**lower panels of Fig. 5, a-d**). In association, ENSO-induced Rossby wave trains, such as the Pacific North America (PNA) and South Pacific America (PSA) teleconnection patterns, are projected to shift eastward[7,113-120] (**upper panels of Fig. 5, a-d**), despite uncertainties in early generations of CMIP models[121,122]. The large deepening/shallowing of the North Pacific trough in the PNA teleconnection is likely to attain a stronger sensitivity to CP SST anomalies than to EP SST anomalies under greenhouse warming[116] (**Fig. 5c, d**).

These projected changes have important climatic implications for affected regions. For example, as the ENSO-induced PNA pattern shifts eastward, El Niño-induced rainfall anomalies are expected to intensify on the west coast of North America, and El Niño–induced surface warming to expand eastward to occupy all of northern North America[113]. As a consequence, many regions affected by ENSO in the present climate are likely to experience more intense ENSO-driven rainfall variability in the future[123].

In addition, due to increased mean-state moisture and increased ENSO variability under greenhouse warming, the asymmetric atmospheric response between El Niño and La Niña are expected to increase[115,120]. As a result, over many land areas, there will be a robust increase in

the spatial extent of ENSO teleconnections during austral summer in both temperature and precipitation[124], leading to an increased impact in El Niño-induced droughts[125,126]. Furthermore, the projected increase in El Niño amplitude provides more favorable large-scale conditions for tropical cyclone formation in the tropical Pacific[127,128] such that island states, such as Fiji, Vanuatu, Marshall Islands, and Hawaii, are likely to see a larger number of tropical cyclones during El Niño events and reduced occurrences during La Niña events in the future[128].

Mechanism and processes influencing ENSO projection

The increase in ENSO SST variability is underpinned by a stronger air-sea coupling arising from an intensification of the equatorial Pacific upper-ocean stratification[29]. The enhanced stratification is caused by surface-intensified warming due to increasing greenhouse gas-induced radiative forcing and freshening owing to increased precipitation, enhancing the response of the surface mixed-layer to a given wind forcing[29,64-67]. Thus, the projected increase in ENSO SST variability is independent of faster warming in the eastern equatorial Pacific than the west, a trend that underpins the projected increase in ENSO rainfall variability[21]. Although models with stronger warming in the eastern equatorial Pacific do tend to generate a greater increase in ENSO SST variability, and vice versa[95,97,129], the greater warming can result from rectification of the increased ENSO SST variability onto the mean state[96,97]. Nevertheless, many factors affect the projection, such as interannual inter-basin interactions, internal variability, and a too-cold equatorial Pacific cold tongue, as discussed below.

Inter-basin interactions

A strong appreciation has formed (**Fig. 1**, by 2019) that on interannual time scales, Atlantic Niña with an anomalous cooling in the equatorial east Atlantic is conducive to a Pacific El Niño[130,131], and an anomalous warming over the tropical North Atlantic may trigger a Pacific La Niña[132], whereas an Indian Ocean basin-wide warming can contribute to a transition from El Niño to La Niña[133]. The majority of models underestimate these remote impacts on ENSO[134-138], with implications on ENSO projections[34,139].

Under greenhouse warming, projected slower warming in the Atlantic Ocean than the Pacific, due to a weakened oceanic heat transport from the South Atlantic induced by a weakened Atlantic Meridional Overturning Circulation[140], can reduce the ability for Atlantic variability to influence ENSO events, as convection is overall skewed toward the Pacific sector[136]. In addition, under greenhouse warming tropical North Atlantic SST anomalies decay faster due to stronger thermal damping in a warmer climate[137], and tropospheric stability increases as the lower atmosphere warms less than the upper troposphere[138], both acting to decrease the forcing of Atlantic variability on ENSO. This scenario contrasts to what has occurred in the post-1980 period, in which the Atlantic has exhibited rapid warming[85,141] with more biennial ENSO variability[142].

448 Although there is no inter-model consensus on how interactions between ENSO and Indian
449 Ocean variability will change under greenhouse warming[143], the inter-basin warming
450 contrasts may vary with time, inducing non-unidirectional projected changes in ENSO, as
451 previously demonstrated in the case of a projected relative warming between the Pacific and
452 the Indian Ocean[53]. However, the impact of the Atlantic and Indian Ocean future warming on
453 future ENSO is likely to be underestimated in climate models, because the simulated present-
454 day inter-basin interactions are underestimated[30,34,85,89].

455 ***Internal variability***

456 It is also realised that ENSO projections are influenced by internal variability (**Fig. 1**, by
457 2020). ENSO variability and its future change differ vastly across ensemble members in a
458 single model under the same emission scenario due to internal variability, for example,
459 arising from small random perturbations to the same initial condition[35-38]. The inter-member
460 spread of future ENSO variability is not completely random, but dependent on past ENSO
461 behaviour: greater initial variability over a multi-decadal period being associated with smaller
462 future variability[35]. Because of greater El Niño amplitude than that of La Niña, ocean-to-
463 atmosphere net heat loss during El Niño events is greater than heat gain during La Niña
464 events[144,145]. The asymmetric heat flux results in a cumulative heat loss that is greater in
465 experiments with initially stronger ENSO variability, causing the thermocline to shoal in the
466 upper western Pacific and deepen in the eastern Pacific initially. Over time, the cumulative
467 heat loss leads to a cooling in the upper central and eastern equatorial Pacific. The cooling
468 partly offsets the greenhouse-forced upper-ocean stratification, such that initially strong
469 ENSO variability tends to be associated with future weak ENSO variability[35].

470 Such relationships are also seen in models with higher ENSO nonlinearity tending to project
471 weaker Niño3.4 variability and a reduced eastern equatorial Pacific warming[48]. As
472 greenhouse gas concentrations increase further, the impact of internal variability relative to
473 the effect from greenhouse-induced change is expected to decrease, and uncertainty in the
474 projections is expected to be dominated by inter-model differences from the 2040's onward[141].

475 ***Impact from the cold-tongue bias***

476 Assessment of ENSO response mechanisms is affected by persistent model biases, of which
477 the common equatorial Pacific too-cold cold-tongue and too-west extension (**Fig. 3d**) is
478 suggested to have impact on ENSO simulation and projected ENSO changes[147]. For instance,
479 the too-cold equatorial eastern Pacific cold tongue can lead to a spuriously weak Bjerknes
480 feedback that, despite being typically offset by a too-weak thermal damping[148,149,150], can
481 hamper simulation of realistic ENSO asymmetry[97] as warm anomalies are harder to grow to
482 establish atmospheric deep convection[150]. While model selection based on realistic ENSO
483 asymmetry is used for ENSO projections, the asymmetry in selected models is still low
484 compared to the observed[35,97].

485 To summarise, although uncertainties remain, a scenario of increased ENSO SST variability
486 with more frequent ENSO SST extremes continues to emerge, with intensified ENSO

teleconnections. Thus, there are multiple lines of evidence indicating that ENSO can be sensitive to climate change. Below we synthesize findings of ENSO sensitivity to past climate change using proxy-based climate reconstructions to provide a historical perspective of changing ENSO.

Paleoclimatic context of ENSO changes

Tropical Pacific interannual variability has been a feature of the Earth's climate system for millions of years[151]. As such, assessments of forced changed in ENSO properties have been carried out in the context of changes in Earth's orbit, volcanic eruptions, and greenhouse gas forcing, as captured in both paleoclimate datasets, observational data, and climate models. This section summarises new advancements of our understanding of ENSO response to past climate forcings that might improve our understanding of its response to future anthropogenic forcings, such as greenhouse gases and aerosols.

Mean circulation and ENSO

External paleoclimate forcings alter the mean state of the tropical Pacific, including the mean surface temperature and its zonal and meridional gradients, surface wind patterns, the depth of the thermocline, the magnitude of the annual cycle, and background noise. However, comparison across periods finds no stable relationship in simulated climate between ENSO variability and many mean circulation features. Since each past climate can be characterized by multiple changes which can be coupled, it is often challenging to separate their role in influencing ENSO variability in proxy records and model simulations alike.

Recent analysis of foraminifera from the eastern equatorial Pacific showed that in the Pliocene weaker ENSO was associated with weaker zonal SST and vertical temperature gradients[152], in agreement with modelling studies[153,154,155]. Last Glacial Maximum reconstructions have corroborated the association of a weaker zonal SST gradient with weaker ENSO variability[156], opposing interpretations from other proxy data that were confounded by changes in the eastern Pacific seasonal SST cycle[157,158,159], as discussed in REF.[160]. Paleoclimate Model Intercomparison Project phase 3 and 4 (PMIP3 and PMIP4) model experiments show no clear relationship between ENSO variance and zonal SST gradient (**Fig. 6a, b**) or mean SST (**Fig. 6c**). The lack of a clear relationship is also true when the climate system has not reached equilibrium, for example, last millennium simulations and proxy synthesis[161] show that models that best simulate modern tropical Pacific climate frequently have a stronger ENSO SST variance when the west-minus-east mean SST contrast is weaker, and vice versa, potentially as a result of ENSO rectification on the mean state[162,163]. However, there is vast diversity in the strength and direction of this relationship, suggesting that it is not constant through time[164], and is likely controlled by multiple mechanisms[161].

Reconstructed temperature variability at the equatorial Pacific during Last Glacial Maximum and Pliocene suggests that ENSO strength is tied to the mean thermocline depth of the eastern equatorial Pacific and the strength of the thermocline feedback[152,156,165]. Modelling studies support the idea that changes in ENSO variance during the mid- and early Holocene and

Pliocene can be attributed to the vertical ocean structure in the central and east equatorial Pacific[155,166,167,168].

Overall, coupling of the zonal, meridional and vertical gradients, the lack of clear relationship between changes in many mean circulation features and ENSO variability in paleoclimate records and model experiments, and the fact that many of the available climate proxies resolve equilibrium conditions rather than transient response to external forcings, make it challenging to the use of any one of the past climates as analogues or reverse-analogue for centennial-scale anthropogenic climate change.

Orbital forcing and ENSO

Changes in Earth's orbital characteristics modulate the seasonal amplitude of solar radiation, generating changes in the mean climate and inducing seasonal shifts in temperature and winds in the tropical Pacific, potentially influencing ENSO properties. General circulation models forced with different orbital conditions simulate on average a 30-40% suppression of the seasonal cycle amplitude of eastern tropical Pacific SST variability during the mid-Holocene (6,000yrs ago) and a weak (10-20%) suppression of ENSO variability[105,169], but large internal variability and inter-model spread challenge the robustness of these conclusions (**Fig. 6a, d**). In the last interglacial, when orbital forcing was similar to that in mid-Holocene forcing but stronger, models show a correspondingly larger decrease in ENSO variance (**Fig. 6a**) in agreement with limited coral records[170]. The simulated orbital sensitivity of ENSO stands in contrast to findings from paleoclimate reconstructions of ENSO variability, which show intervals of reduced ENSO variance that are not in phase with orbital changes in equatorial insolation[166,171]. The simulated magnitude of the annual cycle in the last interglacial is not distinguishable from historical simulations (**Fig. 6d**), challenging the notion of a positive correlation between ENSO variance and annual cycle magnitude[59].

Spanning the last 7,000 years, ENSO proxy-based reconstructions show no clear orbitally forced trend in ENSO variability since the mid-Holocene. Instead, there appears to be a pronounced reduction in ENSO variability and the magnitude of the seasonal cycle between 3,000-5,000 years ago[58,172], a period which does not coincide with any known external forcings. On the contrary, single foraminiferal records[173] and ENSO-related hydroclimate proxy records from lakes and speleothems[174-178] show significant changes in ENSO variance under orbital forcing, in agreement with ENSO sensitivity to orbital forcing in paleoclimate model experiments but several times of magnitude higher than the changes found in these experiments, sometimes of opposite direction[59].

Some of the model-proxy discrepancies can be reconciled by considering changes in ENSO flavours and their different teleconnection patterns[167,179]. For example, the mid-Holocene ENSO reduction was most pronounced in the eastern equatorial Pacific, whereas CP ENSO events remained relatively unaffected or even slightly increased[167]. Given the model uncertainties as well as the discrepancy between paleo-climate reconstructions and model

simulations, it appears that ENSO's sensitivity to orbital forcing remains highly uncertain[59].

Volcanic forcing and ENSO

The impact of strong volcanic forcing on ENSO variability in the past also remains an open question; an answer to this question can improve our understanding of the role of natural and anthropogenic aerosols in ENSO variability in present and future climates[180]. Some model and proxy studies suggest an increase in the probability of El Niño events in the year following an eruption[27,181-185], whereas others show a weak La Niña response[186,187], or no clear response[188,189,190]. Multiple factors are involved, including the Pacific-wide initial conditions, and the location and season of the eruption and the spatial structure of the volcanic aerosols[191-195]. For example, the impact of tropical eruptions on ENSO is modelled to enact via movement of the inter-tropical convergence zone and extratropical teleconnections and northern hemisphere tropical eruptions generate an El Niño-like response. Conversely, southern hemisphere tropical eruptions induce a La Niña-like response[194], as does a uniform negative radiative forcing over the tropics contrary to the expectation from the ocean dynamical thermostat mechanism[80]. Thus, reducing proxy dating uncertainties and accounting for the latitude and timing of eruptions is important for assessing ENSO's sensitivity to aerosol forcing.

In summary, given the short length of the instrumental record, paleoclimate reconstructions and model experiments are critical for understanding ENSO response to external climate forcing, especially in the context of the sensitivity of ENSO feedbacks to changes in the mean state[105,167]. In particular, paleoclimate records appear to show a causal connection between the equatorial Pacific vertical temperature stratification and ENSO strength. However, limitations of paleoclimate records exist[59], arising from many factors including nonlinearities and non-stationarity in teleconnected proxy records[196], subsampling natural ENSO variability, and difficulty in separating the impacts of ENSO, its diversity and seasonal cycle changes in both direct and teleconnected/indirect ENSO proxies. Further, most of these proxy records reflect ENSO-related temperature, rainfall and salinity, which can lead to nonlinearities and non-stationarity in the recorded signal[196]. In addition, regional topography and mesoscale circulation processes can lead to departure of regional signals from the expected large-scale signature of ENSO events[197]. Thus, the observed interannual variance in land-based hydroclimate or coral-based records likely reflect a change in ENSO-related temperature and hydrological variability combined, ENSO diversity and the regional or large-scale teleconnections[167,179,198]. Despite the limitations, paleoclimate reconstructions, when carefully combined with dynamical understanding, offer the ability to groundtruth model simulations and to inform targeted experiments for distinguishing underlying mechanisms.

Conclusions, uncertainties, and prospects

There is an emerging inter-model consensus among models capturing the distinction between EP and CP ENSO events, stronger in CMIP6 than CMIP5, that ENSO SST variability at the

unique centres in each model is likely to increase, leading to an increase in frequency of extreme El Niño and extreme La Niña events in terms of SST anomaly magnitude. Associated with the increase in ENSO SST variability, the equatorial Pacific rainfall response to ENSO intensifies and shifts eastward, as do extratropical teleconnections, leading to stronger climate impacts in the future. There are also increasing lines of paleoclimatic evidence that ENSO variability has increased since the 1950s compared with past centuries, and that ENSO variability strength on long timescales increases with the equatorial Pacific vertical temperature gradient, consistent with the emerging consensus on increased ENSO variability under greenhouse warming. In addition, future changes in ENSO SST are not simply a function of emission scenarios but are influenced by the past history of ENSO variability.

However, uncertainties remain. On multi-decadal timescales, the disparity between the projected weakening in west-minus-east zonal SST gradient and the observed strengthening over the past several decades[31,32,33,81], the too-west and too-cold equatorial Pacific cold tongue, and the too-weak inter-basin interactions[30,34,89,90], reduce confidence in the projected change. On interannual time scales, simulated inter-basin teleconnections are also too weak, leading to a weaker ENSO impact on the Atlantic Niño/Niña, tropical North Atlantic and Indian Ocean SST variability; in turn, their feedbacks on ENSO are too weak[135,137,138]. It is not clear how these two-way interactions will change and how the changes will affect ENSO.

Further, ENSO is coupled with and influenced by other variability at higher latitudes of the Pacific. For example, El Niño events are preceded by and coupled with warm anomalies of the North Pacific meridional mode[199,200,201] and forced by southerly jets from southwestern Pacific[202]. We have incomplete knowledge of how these tropical-extratropical connections are simulated in climate models and how they will respond to greenhouse warming.

In terms of ENSO properties, we know little about how other essential characteristics of ENSO may change, such as the termination and onset of ENSO events, coupling between stochastic noise and ENSO, and interactions between ENSO and the annual cycle[13,59]. In terms of ENSO physics, the role of eddy-induced oceanic heat transport and oceanic turbulent mixing is not well understood or parameterised[203], nor are sub-grid atmosphere process such as atmospheric convection, cloud formation and their coupling to other ENSO processes[204].

Nevertheless, coordinated community efforts like CMIP and advances in computational power will continue to facilitate progress. Large-ensemble simulations[205], long control climate simulations, and high-resolution climate modelling (e.g., 0.1° in horizonal resolution for the ocean model component) show great promise in addressing key questions about ENSO in a warmer world, example of which we highlight further below.

When the "signal" of increased ENSO SST variability or the changing mean state may clearly emerge from the background noise of internal variability, or whether such a signal will ever be detectable in a single realization of the real world, is an open question that is largely unexplored. Long multi-century control simulations of the climate system provide a wide range of realizations for this assessment. The concept of the 'Time of Emergence' for SST and precipitation signals in the equatorial Pacific, referenced to pre-industrial conditions, indicate when it should be possible to detect these signals against the background noise of natural internal variability[206]. For changes in mean SST in Niño3.4 region under the most aggressive greenhouse gas emission scenario, the time of emergence should have been

around the turn of the 21st century (**Fig. 7a**). However, the discrepancy between models and observations and the inter-model spread mean that we have not been able to conclude with confidence that we have observed a clear greenhouse gas forced mean-state temperature change. For changes in mean precipitation in the Niño3.4 region, the signal may not emerge until mid-21st century. Conversely, however, the situation for SST and precipitation variability is reversed, with the rainfall variability emerging sooner than the SST variability (**Fig. 7b**). The earlier emergence of rainfall variability confirms the robust signal of more extreme El Niño events in the future when measured by a rainfall threshold[21]. These results suggest that ENSO changes should be detectable within the 21st century; however, the time of emergence for teleconnections impacting ENSO-affected regions awaits investigation.

Large ensemble experiments within a single model have led to a realization that internal variability[36,37] and butterfly effect influence projected ENSO change. Available simulations suggest that while responding to greenhouse warming, ENSO constantly self-regulates in accordance with its own past behaviour. That is, high past variability takes heat out of the upper equatorial Pacific Ocean, off-setting greenhouse warming-induced upper ocean stratification and weakening ENSO's response, which in turn sets up for a strong subsequent response by reducing oceanic heat loss[35]. The self-regulation raises an issue of whether there is a deterministic equilibrium ENSO response to greenhouse warming in a single realization. In other words, is ENSO change quantifiable in a given window of time in the future? Large ensemble experiments with multiple models offer an opportunity to test the robustness of this self-regulating behaviour and to inspire theoretical models of the associated process.

Furthermore, high resolution climate models not only better resolve ENSO teleconnection patterns, intensity and associated climate extremes at regional scales, subgrid ocean and atmosphere process, but also allow explicit definition of previously unresolved physical processes. One example is heat transport induced by equatorial Pacific oceanic eddies (such as tropical instability waves) on the mean state heat balance of the equatorial Pacific. For the equatorial Pacific mean state, eddy-induced heat transport represents a substantial heat source comparable to heat uptake from the atmosphere[207]. The eddy-induced heat source is reduced during El Niño but increases during La Niña, constraining ENSO amplitude[208] while substantially contributing to ENSO irregularity and predictability[203]. Given that such eddy effects are not resolved by low-resolution climate models, it is likely that the simulated cold tongue bias[209] and other ENSO property biases[148] in CMIP models could be in part due to the absence of the eddy process. Thus, high-resolution ENSO modelling offers a path forward for substantial improvement in ENSO simulations and projections.

To conclude, despite rapid progress over the past five years the issue of ENSO response to greenhouse warming is far from resolved, and many fundamental questions remain. The coming decade offers opportunities for substantial advances as community efforts strengthen, cutting-edge ideas emerge, and realistic models become available. The robust scientific process, whereby debates inspire research and progress identifies new issues, will propel the field forward.

Figures and captions

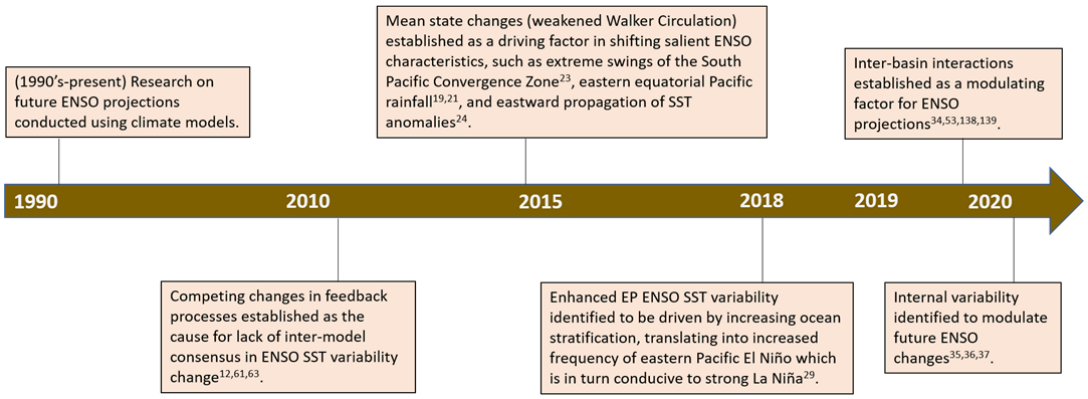

Figure 1 | Timeline of development in understanding ENSO response to greenhouse forcing. Each development is marked at an approximate time and is a result of studies and multiyear-long effort starting in the 90's when climate models were first used to study ENSO future projections[17,18].

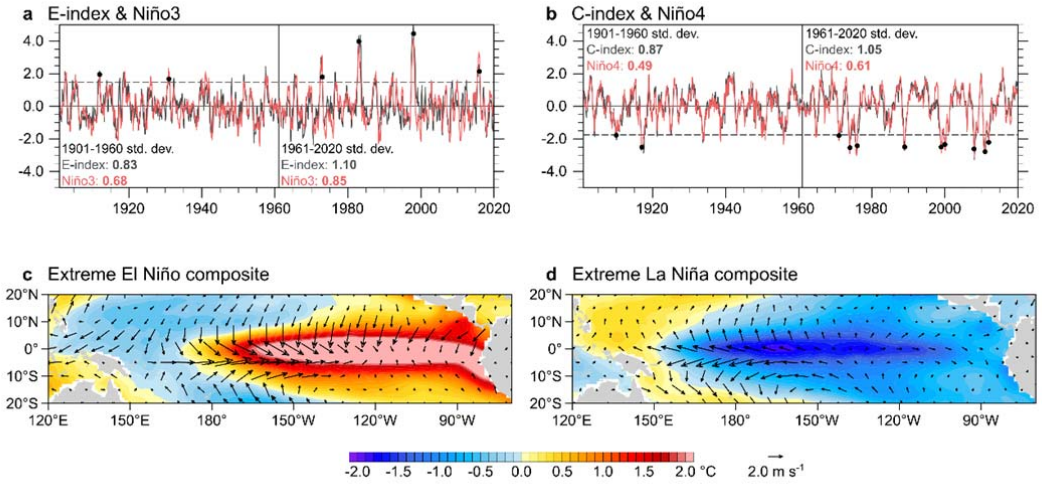

Figure 2 | Observed normalized Niño3 and Niño4 indices and their representation using E-index and C-index. Shown are based on average across three products[68,69,70] from 1901 to 2017. a, b, Niño3 and Niño4 timeseries plotted with E-index and C-index for EP-ENSO and CP-ENSO, respectively. The numbers in each panel indicate the standard deviations of the indices, with the numbers representing the 1901-1960 and 1961-2017 periods. c, d, SST and surface wind composite anomalies for extreme El Niño events defined as when DJF mean E-index >1.5 s.d. (black dots in a), and for extreme La Niña defined as when DJF mean C-index

< -1.75 s.d. (black dots in b), respectively. Anomaly centres for extreme El Niño and extreme La Niña are in the eastern and central equatorial Pacific, respectively. Increased variability of Niño3 or E-index in the post-1960 period is characterised by an increased frequency of extreme El Niño, and increased variability in Niño4 or C-index in the post-1960 period is characterised by an increased frequency of extreme La Niña.

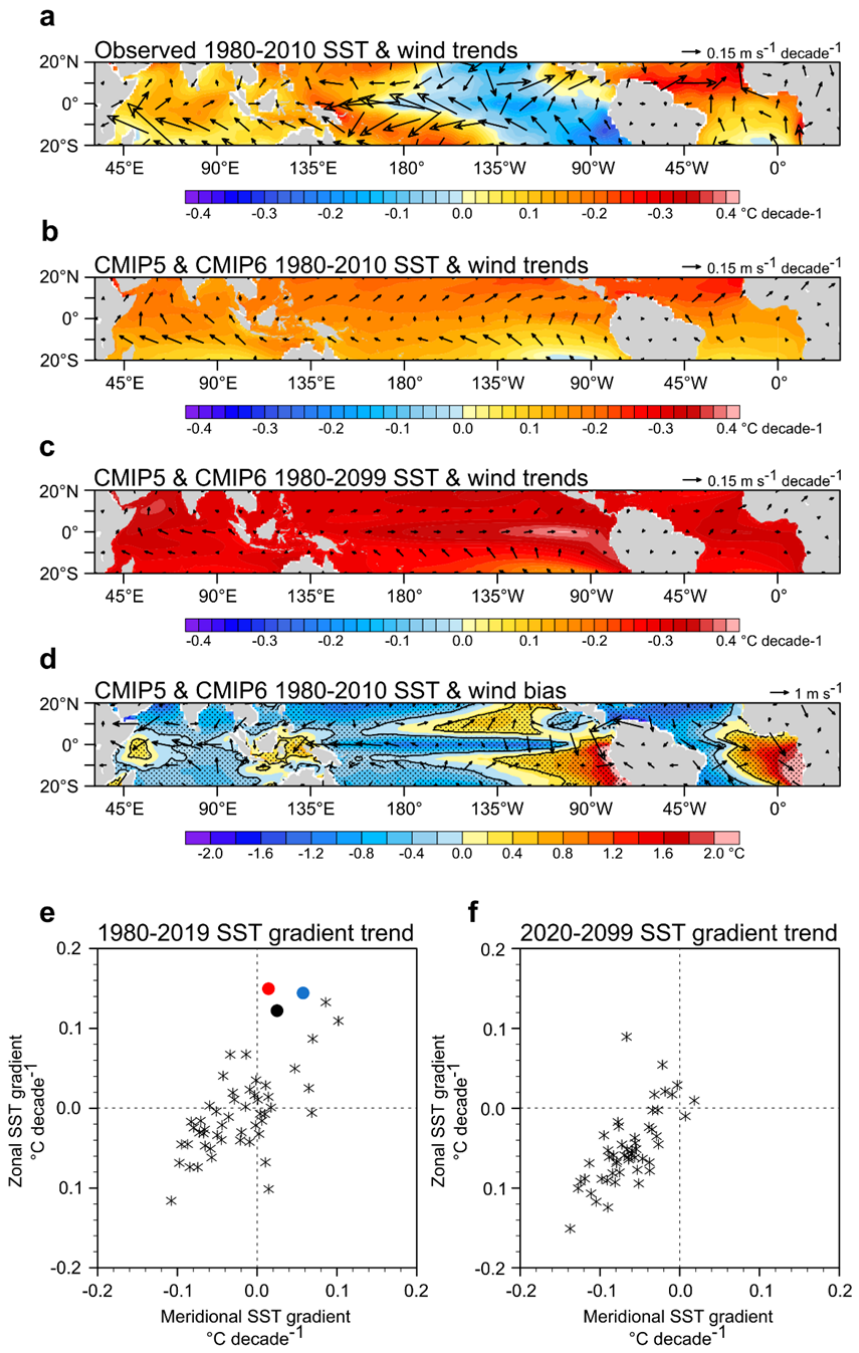

Figure 3 | Observed and simulated tropical Pacific mean state and change. **a**,1980-2010 trends for reanalysis SST[68,69,70] and surface winds[71,72,73]. **a,** As in **b**, but for the average over 28 CMIP5 and

23 CMIP6 models. These models are forced by historical forcing and the representative concentration pathway 8.5 (RCP8.5) emission scenario, or the equivalent, the shared socioeconomic pathway 5-8.5 (SSP5-8.5). **c**, Average SST trends over 28 CMIP5 and 23 CMIP6 models for the 1980-2099. **d**, CMIP5 and CMIP6 mean SST and surface wind bias relative to the observations for the 1980-2010 period. Stippling and black contour indicate the 90% and 95% confidence levels respectively using a two-tailed *t*-test. **e**, Linear trend values over the 1980-2019 period of December-February (DJF) zonal SST gradient and eastern Pacific meridional SST gradient for the 51 CMIP 5/6 models (stars), and three reanalysis datasets[68,69,70] (colour filled circles). Zonal SST gradient is defined following REF.[81] except sign-reversed, that is, the eastern Pacific (5°S-5°N, 180°E-80-°W) area average SST is subtracted from the western Pacific (5°S-5°N, 110°E-180°E) area average SST. The eastern Pacific meridional SST gradient is defined as the areal average off-equatorial northern SST (5°N-10°N, 90°W-150°W) and the southern SST (5°S-10°S, 150°W-90°W) minus the equatorial SST (2.5°S-2.5°N, 90°W-150°W). **f,** As in **e**, for the 2020-2100 period in the CMIP5/6 models. Models suffers from a cold tongue bias and the observed trend over the past decades is within the inter-model range of trends over the same period, but opposite to the long-term trend in majority of models.

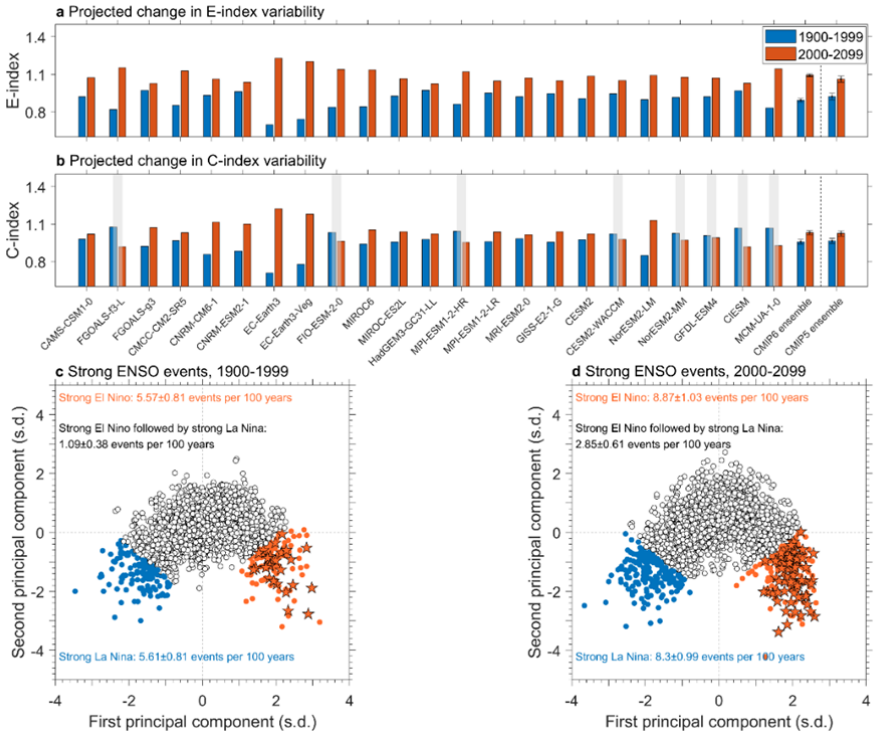

Figure 4 | Projected increase in ENSO SST variability in CMIP6 models. Shown are from 23 CMIP6 models selected based on their ability to simulate ENSO nonlinearity at least 50% of the observed, as indicated by the nonlinear relationship between the first and second principal components of SST variability in the tropical Pacific[29]. These models are forced by historical forcing up to 2014 and thereafter the shared socioeconomic pathway 5-8.5 (SSP5-8.5), the equivalent to the representative concentration pathway 8.5 (RCP8.5) emission scenario. **a,** DJF E-index standard deviation over the present day (1900-1999) and future (2000-2099) periods. All models project increased EP-ENSO variance. **b,** As in **a** but for the C-index. Models simulating a variance reduction

are greyed out. The multi-model mean for the CMIP6 models, and 17 CMIP5 models using in REF.[29] are shown in a and **b**, with error bars indicating one standard deviation value of 10,000 realizations in a Bootstrap test. **c,** Relationship between the first and second principal component for identification of extreme ENSO events. **Orange** dots indicate **extreme El Niño** events (E-index > 1.5 s.d.), and **blue** dots indicate **extreme La Niña events** (C-index <= -1.75 s.d.). **Orange** pentagrams indicate **extreme El Niño** events **followed by an extreme La Niña** event the following year. The corresponding average frequency is labelled in each panel with 90% confidence interval based on a Poisson distribution. A stronger inter-model consensus on increased ENSO SST variability emerges in CMIP6 than CMIP5 models.

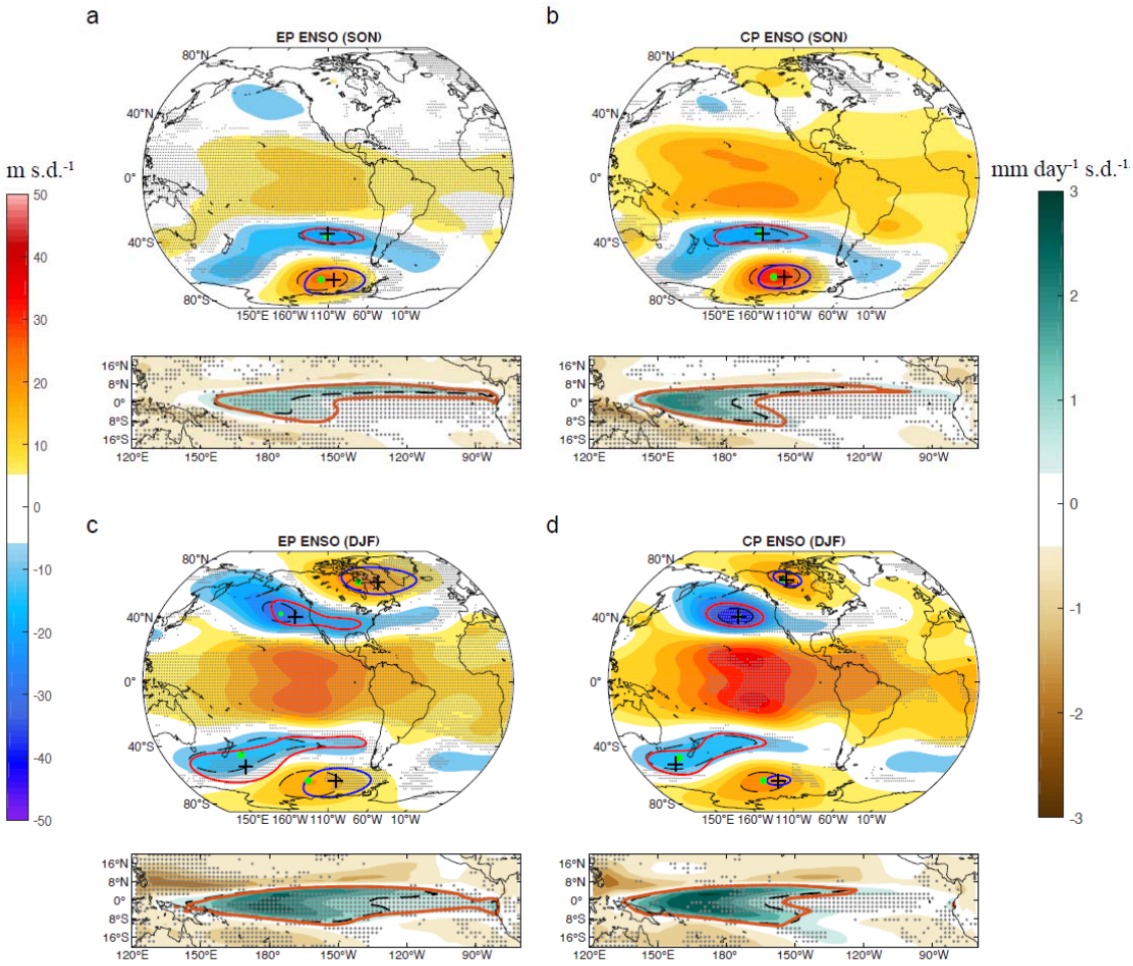

Figure 5 | Changing ENSO teleconnections under greenhouse warming. The results are based on CMIP6 models forced by historical forcing up to 2014 and thereafter the shared socioeconomic pathway 5-8.5 (SSP5-8.5) emission scenario. Shown are simultaneous regressions of quadratically detrended 200hPa geopotential height (m s.d.$^{-1}$) and rainfall anomalies (mm day^{-1} s.d.$^{-1}$) onto **a**, **b,** normalized E-index and C-index for SON, and **c, d**, for DJF. Regression coefficients for the present-day period (1900-1999) are shaded in colour. The centres of the PSA or the PNA (upper part of each panel) for the **present-day** climate are indicated by a **dashed** contour surrounding a **green dot**, and for the **future** climate a **solid** contour of the same value surrounding a **cross** for each centre; the 1 mm day^{-1} s.d.$^{-1}$ rainfall anomalies (lower part of each panel) is plotted in **black dashed** contour for **the**

present-day and **solid red** for the **future** (2000-2099) period. Results are for SON and DJF when the PSA and PNA peaks, respectively. Stippling indicates an inter-model consensus with more than two thirds of models showing same-signed response. The PSA and PNA centres during EP-ENSO are situated more to the east than during CP-ENSO, and these centres tend to either strengthen or shift eastward under greenhouse warming, particularly in the ENSO mature season of DJF.

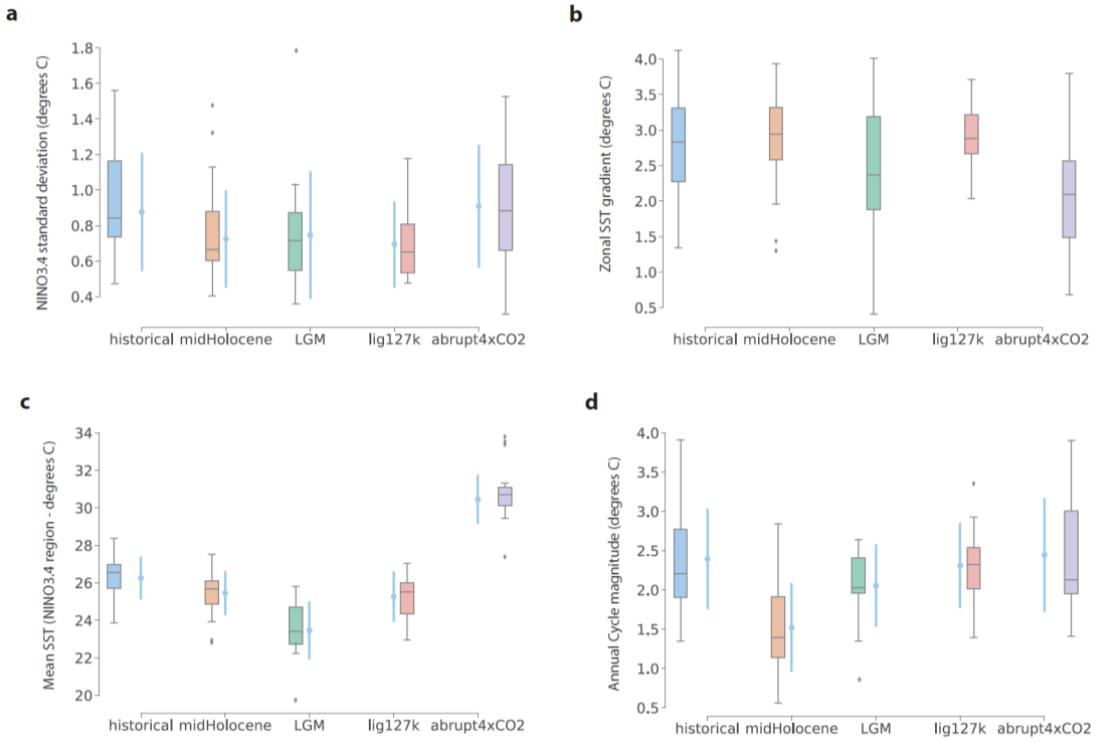

Figure 6 | Tropical Pacific mean state and ENSO variability in past climate. Shown are simulations with PMIP3/CMIP5 and PMIP4/CMIP6 models as described in REF.[105]: historical, mid-Holocene, Last Glacial Maximum (LGM), last interglacial (lig127k) and abrupt 4xCO2 for **a**, Niño3.4 variability, **b**, west-minus-east SST gradient, **c**, mean SST, and **d**, annual cycle magnitude in the Niño3.4 region. All the paleoclimate simulation outputs have been calendar-adjusted using the PaleoCalAdjust tool[210]. The magnitude of the annual cycle is defined as the range of monthly climatological SST in the Niño3 region (5°S-5°N, 150°W-90°W), and the zonal SST gradient as the West (5°S-5°N, 100°E-180°E) minus East Pacific (5°S-5°N, 160°W-80°W) annual mean SST difference. **Boxplot**s indicate **intermodel** spread, and light blue pointplots indicate the spread when including internal variability estimated using 100 random 50-yr samples from each model simulation (error bars draw the standard deviation of samples). While models agree on lower ENSO variance in past climates than the present-day climate, its relationship with the annual cycle, zonal SST gradient and mean SST in the central and eastern Pacific shows vast diversity in the strength and direction.

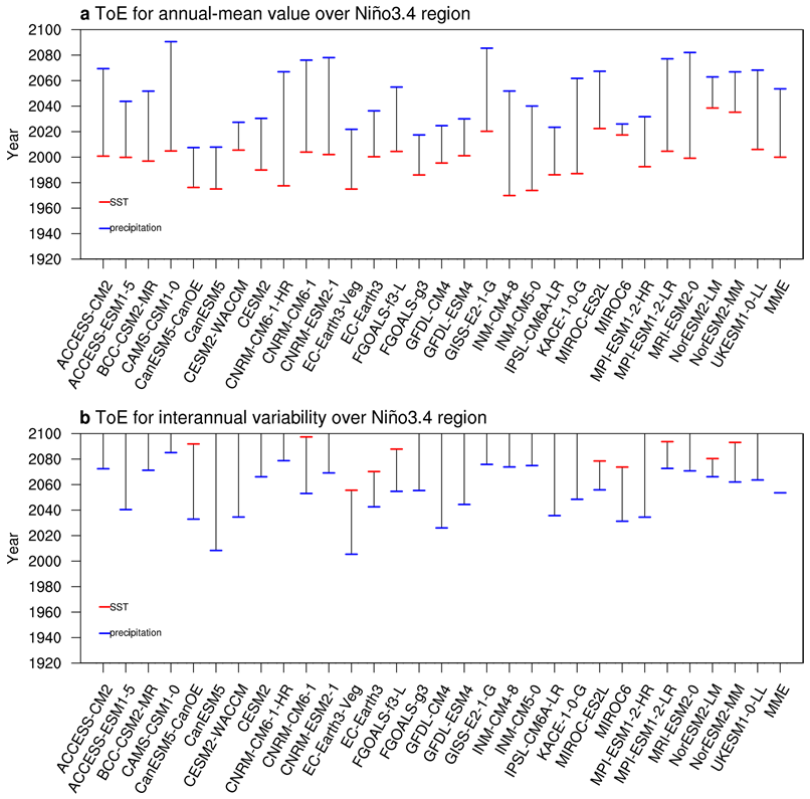

Figure 7 | Time of emergence (ToE) of climate change signals. Signals are sought from outputs of each CMIP6 model under historical forcing and shared socioeconomic pathway 5-8.5 (SSP5-8.5) emission scenario over the 1850 to 2099 period (150 years), and "noise" is diagnosed from a 500-year pre-industrial (piControl) experiment of the respective model as the standard deviation of annual-mean values. **a,** ToE for annual-mean **SST** in **Red** and **rainfall** in **blue,** both averaged over the Niño3.4 region, is provided as year when signals emerge from noise, for each model and for the multi-model ensemble (MME) mean. To obtain evolution of the signal, we regress timeseries of 150 annual mean values in each grid point onto a smoothed version of the tropical-mean (30°S-30°N) by fitting a fourth-order polynomial[206]. ToE is defined as the year when the signal-to-noise ratio exceeds 1. **b**, ToE for interannual variability is given as the end year of a 30-year window over which running standard deviation of annual mean anomalies is calculated. Evolution of the signal is obtained by regressing time series of 30-year running standard deviation of anomalies quadratically detrended for each 30-year period onto time series of 30-year running climatology of the tropical mean similarly smoothed by fitting a fourth-order polynomial. For illustration, ToE for interannual variability is defined as when the signal-to-noise ratio exceeds 1.5. The ToE for interannual rainfall variability is sooner than that for interannual SST variability, whereas the ToE for the annual-mean rainfall is later than annual-mean SST.

References

1. Philander, S. G. H., Yamagata, T., & Pacanowski, R. C. Unstable air-sea interactions in the tropics. *J. Atmos.* **41**, 604–613 (1984).
2. Ropelewski, C. F. & Halpert, M. S. Global and regional scale precipitation patterns

associated with the El Niño/Southern Oscillation. *Mon. Wea. Rev.* **115**, 1606–1626 (1987).
3. McPhaden, M. J., Zebiak, S. E., & Glantz, M. H. ENSO as an integrating concept in earth science. *Science*, **314**, 1740-1745 (2006).
4. L'Heureux, M. L. et al. Observing and predicting the 2015/16 El Niño. *Bull. Am. Meteorol. Soc.* **98**, 1363–1382 (2017).
5. Santoso, A., McPhaden, M. J., & Cai, W. The defining characteristics of ENSO extremes and the strong 2015/16 El Niño. *Rev. Geophys.* **55**, 1079-1129 (2017).
6. Bjerknes, J. Atmospheric teleconnections from the equatorial Pacific. *Mon. Weather Rev.* **97**, 163-172 (1969).
7. Cai, W. et al. Climate impacts of the El Nino-Southern Oscillation on South America. *Nature reviews earth & environment* **1**, 215-231 (2020).
8. Ashok, K., Behera, S. K., Rao, S. A., Weng, H. Y. & Yamagata, T. El Niño Modoki and its possible teleconnection. *J. Geophys. Res.* **112**, C11007 (2007). **Defines a type of El Niño with maximum SST anomaly in the equatorial central Pacific atmospheric teleconnection different from El Niño with anomaly centre in the equatorial eastern Pacific.**
9. McPhaden, M. J., Santoso, A., & Cai, W. (Eds.). El Niño Southern Oscillation in a Changing Climate **253,** *John Wiley & Sons* (2020).
10. IPCC (2013). Climate Change 2013: The Physical Science Basis. Contribution of Working Group I to the Fifth Assessment Report of the Intergovernmental Panel on Climate Change [Stocker, T.F., Qin, D., Plattner, G.-K., Tignor, M., Allen, S.K., Boschung, J., et al. (eds.)]. Cambridge University Press, Cambridge, United Kingdom and New York, NY, USA, 1535 pp
11. IPCC (2018). Global Warming of 1.5°C. An IPCC Special Report on the impacts of global warming of 1.5°C above pre-industrial levels and related global greenhouse gas emission pathways, in the context of strengthening the global response to the threat of climate change, sustainable development, and efforts to eradicate poverty [Masson-Delmotte, V., Zhai, P., Pörtner, H.-O., Roberts, D., Skea, J., Shukla, P.R., et al. (eds.)]. Avaiable from https://www.ipcc.ch/sr15/
12. Collins, M., et al. The impact of global warming on the tropical Pacific Ocean and El Niño. *Nat. Geosci.* **3**, 391-397 (2010).
13. Cai, W. et al. ENSO and Greenhouse Warming. *Nat. Clim. Change* **5**, 849–859 (2015).
14. Jin, F.-F., & Neelin, J. D. Modes of interannual tropical ocean - atmosphere interaction—A unified view. Part I: Numerical results. *J. Atmos.* **50**, 3477–3503 (1993).
15. An, S.-I., & Jin, F.-F. An eigen analysis of the interdecadal changes in the structure and frequency of ENSO mode. *Geophys. Res. Lett.* **27**, 1573–1576 (2000).
16. Fedorov, A. V., & Philander, S. G. A stability analysis of tropical ocean-atmosphere interactions: Bridging measurements and theory for El Niño. *J. Climate* **14**, 3086–3101 (2001).
17. Meehl, G. A., Brantstator, G. W., & Washington, W. M. Tropical Pacific interannual variability and CO2 climate change. *J. Clim*. **6**, 42–63 (1993).

18. Tett, S. Simulation of El Niño - Southern Oscillation-like variability in a global AOGCM and its response to CO2 increase. *J. Clim*. **8**, 1473–1502 (1995).
19. Power, S. B., Delage, F., Chung, C., Kociuba, G., & Keay, K. Robust twenty-first century projections of El Niño and related precipitation variability. *Nature* **502**, 541–545 (2013).
20. Yun, K. S. et al. Increasing ENSO–rainfall variability due to changes in future tropical temperature–rainfall relationship. *Commun. Earth Environ.* **2,** 43 (2021).
21. Cai, W. et al. Increasing frequency of extreme El Niño events due to greenhouse warming. *Nat. Clim. Change* **4**, 111–116 (2014).
22. Wang, G. et al. Continued increase of extreme El Niño frequency long after 1.5C warming stabilization. *Nat. Clim. Change* **7**, 568–572 (2017).
Finds that extreme El Niño frequency continues to increase for up to a century after global warming is halted at 1.5°C above pre-industrial level
23. Cai, W. et al. More extreme swings of the South Pacific convergence zone due to greenhouse warming. *Nature* **488**, 365–369 (2012).
24. Santoso, A. et al. Late-twentieth-century emergence of the El Niño propagation asymmetry and future projections. *Nature* **504**, 126 (2013).
25. Cai, W. et al. Increased frequency of extreme La Niña events under greenhouse warming. *Nat. Clim. Change* **5**, 132–137 (2015).
26. Cobb, K. M. et al. Highly Variable El Nino-Southern Oscillation Throughout the Holocene. *Science* **339**, 67-70 (2013).
27. McGregor, S., Timmermann, A. & Timm, O. A unified proxy for ENSO and PDO variability since 1650. *Clim. Past* **6**, 1-17 (2010).
28. McGregor, H. et al. A weak El Niño/Southern Oscillation with delayed seasonal growth around 4300 years ago, *Nat. Geosci.* **6**, 949–953 (2013).
29. Cai, W. et al. Increased variability of eastern Pacific El Niño under greenhouse warming. *Nature* **564**, 201–206 (2018).
30. Luo, J.-J., Wang, G., & Dommenget, D. May common model biases reduce CMIP5's ability to simulate the recent Pacific La Niña-like cooling? *Clim. Dyn.* **18**, 1-17 (2018).
Proposes the hypothesis that common model biases may favor an El Niño-like warming in response to greenhouse gas forcing in CMIP5.
31. Coats, S., & Karnauskas, K. B. A Role for the Equatorial Undercurrent in the Ocean Dynamical Thermostat, *J. Clim.* **31**, 6245-6261 (2018).
32. Seager, R. et al. Strengthening tropical Pacific zonal sea surface temperature gradient consistent with rising greenhouse gases. *Nat. Clim. Chang.* **9,** 517–522 (2019).
33. Chung, E. S. et al. Reconciling opposing Walker circulation trends in observations and model projections. *Nat. Clim. Chang.* **9,** 405–412 (2019).
Using satellite observations, shows a substantially less strengthening of the Pacific Walker circulation during recent decades in satellite observations than in reanalysis products, and a dominant role of internal variability in the strengthening.
34. Cai, W. et al. Pantropical climate interactions. *Science* **363**, eaav4236 (2019).

35. Cai, W., Ng, B., Geng, T., Wu, L., Santoso, A., & McPhaden, M. J. Butterfly effect and a self-modulating El Niño response to global warming. *Nature* **585**, 68-73 (2020).
Demonstrates that ENSO exhibits a self-regulating behaviour such that ENSO's future variability is shaped by its past, thus modulating the effect of greenhouse forcing.
36. Maher, N., Matei, D., Milinski, S., & Marotzke, J. ENSO change in climate projections: forced response or internal variability? *Geophys. Res. Lett*. **45**, 11-390 (2018).
37. Zheng, X.-T., Hui, C., & Yeh, S. W. Response of ENSO amplitude to global warming in CESM large ensemble: uncertainty due to internal variability. *Clim. Dyn.* **50**, 4019-4035 (2018).
38. Ng, B., Cai, W., Cowan, T., & Bi, D. (2021). Impacts of Low-Frequency Internal Climate Variability and Greenhouse Warming on El Niño–Southern Oscillation, *J. Clim*. ***34***, 2205-2218 (2021).
39. Eyring, V. et al. Overview of the Coupled Model Intercomparison Project Phase 6 (CMIP6) experimental design and organization. *Geosci. Model Dev*. **9**, 1937–1958 (2016).
40. Fu, C. & Fletcher, J. O. Two patterns of equatorial warming associated with El Niño. *Mon. Sci. J.* **30**, 1360-1364 (In Chinese) (1985).
Shows that there are two types of equatorial warming associated with El Niño.
41. Fu, C., Diaz, H. F. & Fletcher, J. O. Characteristics of the response of sea surface temperature in the central Pacific associated with warm episodes of the Southern Oscillation. *Mon. Wea. Rev.* **114**, 1716-1738 (1986).
42. Capotondi, A. et al. Understanding ENSO diversity. *Bull. Am. Meteorol. Soc.* **96**, 921–938 (2015).
43. Capotondi, A., Wittenberg, A.T., Kug, J.-S., Takahashi, K., & McPhaden, M. J. ENSO Diversity. ENSO in a Changing Climate: Challenges, Paleo-Perspectives, and Outlook. *In El Niño Southern Oscillation in a Changing Climate (eds M.J. McPhaden, A. Santoso and W. Cai). AGU Monograph*, (2020)
44. Takahashi, K., & Dewitte, B. Strong and moderate nonlinear El Niño regimes. *Clim. Dyn.* **46**, 1627–1645 (2016).
45. Timmermann, A. et al. (2018). El Niño-southern oscillation complexity. *Nature* **559**, 535-545.
46. Dommenget, D., Bayr, T., & Frauen, C. Analysis of the non-linearity in the pattern and time evolution of El Niño Southern Oscillation. *Clim. Dyn* **40**, 2825-2847 (2013).
47. Takahashi, K., Montecinos, A., Goubanova, K., & Dewitte, B. ENSO regimes: Reinterpreting the canonical and Modoki El Niño. *Geophys. Res. Lett.* **38**, L10704 (2011).
48. Karamperidou, C., Jin, F.-F. & Conroy, J. L. The importance of ENSO nonlinearities in tropical Pacific response to external forcing. *Clim. Dyn.* **49**, 2695–2704 (2017).
49. Lee, T., & McPhaden, M. J. Increasing intensity of El Niño in the central-equatorial Pacific. *Geophys. Res. Lett.* **37**, L14603 (2010).

50. Capotondi, A., & Sardeshmukh, P. D. Is El Niño really changing? *Geophys. Res. Lett.* **44**, 8548–8556 (2017).
51. Wang, B. *et al.* Historical change of El Niño properties sheds light on future changes of extreme El Niño. *Proc. Natl. Acad. Sci.* **116**, 22512-17 (2019).
52. Zhang, Q., Guan, Y. & Yang, H. ENSO amplitude change in observation and coupled models. *Adv. Atmos. Sci.* **25**, 361–366 (2008).
53. Kim, S. T. *et al.* Response of El Niño sea surface temperature variability to greenhouse warming. *Nat. Clim. Chang.* **4**, 786–790 (2014).
54. Geng, T., Cai, W., & Wu, L. Two types of ENSO varying in tandem facilitated by nonlinear atmospheric convection. *Geophys. Res. Lett.* **47**, e2020GL088784 (2020).
55. Kennedy, J. J. A review of uncertainty in in situ measurements and data sets of sea surface temperature. *Reviews of Geophysics* **52**, 1-32 (2014).
56. Li, J. et al. El Niño modulations over the past seven centuries. *Nat. Clim. Change 3*, 822-826 (2013).
57. Liu, Y. et al. Recent enhancement of central Pacific El Niño variability relative to last eight centuries. *Nat. Commun.* **8**, 15386 (2017).
58. Grothe, P. R. et al. Enhanced El Niño–Southern oscillation variability in recent decades, *Geophys. Res. Lett.* **47**, e2019GL083906 (2020)
Shows decreased ENSO variance 3-5,000 years ago and ENSO strengthening in the last five decades, using a new ensemble of fossil coral oxygen isotope records from the central equatorial Pacific.
59. Karamperidou, C. et al. ENSO in a Changing Climate: Challenges, Paleo-Perspectives, and Outlook. *In El Niño Southern Oscillation in a Changing Climate (eds M.J. McPhaden, A. Santoso and W. Cai). AGU Monograph*, (2020).
60. Freund, M. et al. Higher frequency of Central Pacific El Niño events in recent decades relative to past centuries, *Nat. Geosci.* **12**, 450-455 (2019)
61. Philip, S. Y. & van Oldenborgh, G. J. Shifts in ENSO coupling processes under global warming. *Geophys. Res. Letts.* **33**, L11704 (2006).
62. Jin, F.-F., Kim, S. T. & Bejarano, L. A coupled-stability index for ENSO. *Geophys. Res. Lett.* **33**, L23708. (2006).
63. Kim, S. T., & Jin, F.-F. An ENSO stability analysis. Part II: Results from the twentieth and twenty□first century simulations of the CMIP3 models. *Clim. Dyn.* **36**, 1609-1627 (2011).
64. Carréric, A. et al. Change in strong Eastern Pacific El Niño events dynamics in the warming climate. *Clim. Dyn.* **54**, 901 (2020).
65. Dewitte, B., Yeh, S.-W., Moon, B.-K., Cibot, C., & Terray, L. Rectification of the ENSO variability by interdecadal changes in the equatorial background mean state in a CGCM simulation. *J. Clim.* **20**, 2002-2021 (2007).
66. Timmermann, A. et al. Increased El Niño frequency in a climate model forced by future greenhouse warming. *Nature* **398**, 694–697 (1999).
67. Thual, S., Dewitte, B., An, S.-I., & Ayoub, N. Sensitivity of ENSO to stratification in a recharge-discharge conceptual model. *J. Clim.* **4**, 4331-4348 (2011).

Refines theoretical framework showing intensified ocean-atmosphere coupling as the mean upper-ocean stratification increases.

68. Rayner, N. A. et al. Global analyses of sea surface temperature, sea ice, and night marine air temperature since the late nineteenth century, *J. Geophys. Res.* **108**, 4407 (2003).
69. Huang, B. et al. Extended Reconstructed Sea Surface Temperature version 5 (ERSSTv5), Upgrades, validations, and intercomparisons. *J. Clim*, **30**, 8179–8205 (2017).
70. Ishii, M., A. Shouji, S. Sugimoto, & T. Matsumoto. Objective Analyses of Sea-Surface Temperature and Marine Meteorological Variables for the 20th Century using ICOADS and the Kobe Collection. *Int. J. Climatol.* **25**, 865-879 (2005).
71. Slivinski, L. C. et al. Towards a more reliable historical reanalysis: Improvements for version 3 of the Twentieth Century Reanalysis system. *Quart. J. R. Meteorol. Soc.* **145**, 2876-2908 (2019).
72. Poli, P. et al. ERA-20C: An atmospheric reanalysis of the twentieth century. *J. Clim.* **29**, 4083-4097 (2016).
73. Kobayashi, S. et al. The JRA-55 Reanalysis: General specifications and basic characteristics. *J. Meteorol. Soc. Japan Ser. II.* **93**, 5-48 (2015).
74. Lian, T., Chen, D., Ying, J., Huang, P. & Tang, Y. Tropical Pacific trends under global warming: El Niño-like or La Niña-like? *Natl. Sci. Rev.* **5**, 810-812 (2018).
75. Cai, W., et al. ENSO Response to Greenhouse Forcing. *In El Niño Southern Oscillation in a Changing Climate (eds M.J. McPhaden, A. Santoso and W. Cai), AGU Monograph*, (2020).
76. Knutson, T. R., & Manabe, S. Time-Mean Response over the Tropical Pacific to Increased CO_2 in a Coupled Ocean-Atmosphere Model, *J. Clim.* **8**, 2181-2199 (1995).
77. Liu, Z., Vavrus, S., He, F., Wen, N., & Zhong, Y. Rethinking Tropical Ocean Response to Global Warming: The Enhanced Equatorial Warming, *J. Clim*. **18**, 4684-4700 (2005).
78. Xie, S., Deser, C., Vecchi, G. A., Ma, J., Teng, H., & Wittenberg, A. T. Global Warming Pattern Formation: Sea Surface Temperature and Rainfall, *J. Clim.* **23**, 966-986 (2010).
79. Meehl, G. & Washington, W. El Niño-like climate change in a model with increased atmospheric CO_2 concentrations. *Nature* **382,** 56–60 (1996).
80. Clement, A. C., Seager, R., Cane, M. A., & Zebiak, S. E. An Ocean Dynamical Thermostat, *J. Clim.* **9**, 2190-2196 (1996).
81. Watanabe, M. et al. Enhanced warming constrained by past trends in equatorial Pacific sea surface temperature gradient. *Nat. Clim. Chang.* **11,** 33–37 (2021).
82. Kociuba, G., & Power, S. B. Inability of CMIP5 Models to Simulate Recent Strengthening of the Walker Circulation: Implications for Projections, *J. Clim*. **28**, 20-35 (2015).
83. Coats, S., & Karnauskas, K. B. Are simulated and observed twentieth century tropical Pacific sea surface temperature trends significant relative to internal

variability? *Geophys. Res. Lett.* **44**, 9928– 9937 (2017).
84. Zhang, L. et al. Indian Ocean warming trend reduces Pacific warming response to anthropogenic greenhouse gases: An interbasin thermostat mechanism. *Geophys. Res. Lett.* **46**, 10882-10890 (2019).
85. McGregor, S. et al. Recent Walker circulation strengthening and Pacific cooling amplified by Atlantic warming. *Nat. Clim. Change* **4,** 888–892 (2014).
86. Meehl, G.A. et al. Atlantic and Pacific tropics connected by mutually interactive decadal-timescale processes. *Nat. Geosci.* **14,** 36–42 (2021).
87. Li, X., Xie, S.-P., Gille, S. T., & Yoo, C. Atlantic induced pan-tropical climate change over the past three decades. *Nat. Clim. Change* **6**, 275–279 (2016).
88. Lee, S.-K., Kim, D., Foltz, G. R., & Lopez, H. Pantropical response to global warming and the emergence of a La Niña-like mean state trend. *Geophys. Res. Lett.* **47**, e2019GL086497 (2020).
89. McGregor, S. et al. Model tropical Atlantic biases underpin diminished Pacific decadal variability. *Nat. Clim. Change* **8,** 493–498 (2018).
90. Kajtar, J. B., Santoso, A., McGregor, S., England, M. H., & Baillie, Z. Model under-representation of decadal Pacific trade wind trends and its link to tropical Atlantic bias. *Clim. Dyn.* **50**, 1471–1484 (2018).
91. Li, C., Dommenget, D. & McGregor, S. Trans-basin Atlantic-Pacific connections further weakened by common model Pacific mean SST biases. *Nat. Commun.* **11,** 5677 (2020).
92. Stuecker, M. F. et al. Strong remote control of future equatorial warming by off-equatorial forcing. *Nat. Clim. Chang.* **10,** 124–129 (2020).
Demonstrates opposite signed feedbacks in the equatorial and off equatorial regions to greenhouse gas forcing via coupled interactions between clouds, Hadley Circulation, and oceanic subtropical cells.
93. Heede, U. K., Fedorov, A. V., & Burls, N. J. Time Scales and Mechanisms for the Tropical Pacific Response to Global Warming: A Tug of War between the Ocean Thermostat and Weaker Walker, *J. Clim.* 33, 6101-6118 (2020).
94. Cai, W., & Whetton, P. H. Evidence for a time-varying pattern of greenhouse warming in the Pacific Ocean. *Geophys. Res. Lett.* 27, 2577-2580 (2000).
95. Zheng, X.-T., Xie, S.-P., Lv, L. H., & Zhou, Z. Q. Intermodel uncertainty in ENSO amplitude change tied to Pacific Ocean warming pattern. *J. Clim.* 29, 7265–7279 (2016).
96. Kohyama, T., Hartmann, D. L., & Battisti, D. S. La Niña–like Mean-State Response to Global Warming and Potential Oceanic Roles, *J. Clim*. 30, 4207-4225 (2017).
97. Hayashi, M., Jin, F.-F. & Stuecker, M. F. Dynamics for El Niño-La Niña asymmetry constrain equatorial-Pacific warming pattern. *Nat. Commun.* 11, 4230 (2020).
98. Ying, J., Huang, P., Lian, T., & Tan, H. Understanding the effect of an excessive cold tongue bias on projecting the tropical Pacific SST warming pattern in CMIP5 models. *Clim. Dyn.* **52**, 1805–1818 (2018).
99. Taschetto, A. S., Sen Gupta, A., Jourdain, N., Santoso, A., Ummenhofer, C. C., &

England, M. H. Cold tongue and warm pool ENSO events in CMIP5: mean state and future projections. *J. Clim.* **27**, 2861–2885 (2014).
100. Philip, S. Y. & van Oldenborgh, G. J. Shifts in ENSO coupling processes under global warming. *Geophys. Res. Letts.* **33**, L11704 (2006).
101. DiNezio, P. N., Kirtman, B. P., Clement, A. C., Lee, S.-K., Vecchi, G. A., & Wittenberg, A. Mean climate controls on the simulated response of ENSO to increasing greenhouse gases. *J. Clim.* **25**, 7399– 7420 (2012).
102. Dommenget, D., & Vijayeta, A. Simulated future changes in ENSO dynamics in the framework of the linear recharge oscillator model. *Clim. Dyn.* **53**, 4233–4248 (2019).
103. Chen, C., Cane, M. A., Wittenberg, A. T., & Chen, D. ENSO in the CMIP5 simulations: Life cycles, diversity, and responses to climate change. *J. Clim.* **30**, 775– 801 (2017).
104. Wang, G., Cai, W., & Santoso, A. Stronger increase in the frequency of extreme convective El Niño than extreme warm El Niño under greenhouse warming. *J. Clim.* **33**, 675-690 (2020).
105. Brown, J. R. et al. Comparison of past and future simulations of ENSO in CMIP5/PMIP3 and CMIP6/PMIP4 models. *Clim. Past* **16**, 1777–1805 (2020).
106. Zheng, X.-T., Hui, C., Xie, S.-P., Cai, W. & Long, S.-M. Intensification of El Niño rainfall variability over the tropical Pacific in the slow oceanic response to global warming. *Geophys. Res. Lett.* 46, 2253-2260 (2019).
107. Feng, J., Lian, T., Ying, J., Li, J. & Li, G. Do CMIP5 models show El Niño diversity? *J. Clim.,* **33,** 1619-1641 (2020).
108. Lemmon, D. E. & Karnauskas, K. B. A Metric for Quantifying ENSO Diversity with Implications for ENSO–Mean State Interaction. *Clim. Dyn.,* **52**, 7511-7523. doi: 10.1007/s00382-018-4194-3 (2019).
109. Fredriksen, H.-B., Berner, J., Subramanian, A. C., & Capotondi, A. How does El Niño-Southern Oscillation change under global warming-A first look at CMIP6. *Geophys. Res. Lett.* 47, e2020GL090640 (2020).
110. Planton, Y. et al. Evaluating Climate Models with the CLIVAR 2020 ENSO Metrics Package. *Bull. Am. Meteorol. Soc.* **102**, E193-E217 (2021).
111. McKenna, S., Santoso, A., Sen Gupta, A., Taschetto, A., & Cai, W. Indian Ocean Dipole in CMIP5 and CMIP6: Characteristics, biases, and links to ENSO. *Sci. Rep.* **10**, 11500 (2020).
112. Zelinka, M. D. et al. Causes of higher climate sensitivity in CMIP6 models. *Geophys. Res. Lett.* **47**, e2019GL085782 (2020).
113. Zhou, Z.-Q., Xie, S.-P., Zheng, X.-T., Liu, Q. & Wang, H. Global warming-induced changes in El Niño teleconnections over the North Pacific and North America. *J. Clim.* **27**, 9050–9064 (2014).
114. Bonfils, C. J. et al. Relative contributions of mean-state shifts and ENSO-driven variability to precipitation changes in a warming climate. *J. Clim.* **28**, 9997–10013. (2015).
115. Huang P. Time-varying response of ENSO-induced tropical Pacific rainfall to global warming in CMIP5 models. Part II: intermodel uncertainty. *J Clim*. **30**, 595–608 (2017).

116. Chen, Z., Gan, B., Wu, L. & Jia, F. Pacific-North American teleconnection and North Pacific Oscillation: historical simulation and future projection in CMIP5 models. *Clim. Dyn.* **50**, 4379–4403 (2018).
117. Yeh, S.-W. et al. Atmospheric teleconnections and their response to greenhouse gas forcing. *Rev Geophys.* **56,** 185–206 (2018).
118. Michel, C., Li, C., Simpson, I. R., Bethke, I., King, M. P. & Sobolowski, S. The Change in the ENSO Teleconnection under a Low Global Warming Scenario and the Uncertainty due to Internal Variability. *J. Clim.* **33**, 4871-4889 (2020).
119. Sohn, B.-J., Yeh, S.-W., Lee, A. & Lau, W. K. M. Regulation of atmospheric circulation controlling the tropical Pacific precipitation change in response to CO_2 increases. *Nat. Commun.* **10**, 1-8 (2018).
120. Yan, Z., Wu, B., Li, T., Collins, M., Clark, R., Zhou, T., Murphy, J. & Tan, G. Eastward Shift and Extension of ENSO-Induced Tropical Precipitation Anomalies under Global Warming. *Sci. Adv.* **6**, eaax4177 (2020).
121. Stevenson, S. L., Significant changes to ENSO strength and impacts in the twenty-first century: Results from CMIP5. *Geophy. Res. Lett*. **39**, L17703 (2012).
122. Tedeschi, R. G. & Collins, M. The influence of ENSO on South American precipitation: simulation and projection in CMIP5 models. *Int. J. Climatol.* **37**, 3319–3339 (2017).
123. Power, S. B. & Delage, F. P. D. El Niño–Southern Oscillation and Associated Climatic Conditions around the World during the Latter Half of the Twenty-First Century. *J. Clim.* **31**, 6189–6207 (2018).
124. Perry, S. J., McGregor, S., Sen Gupta, A., England, M. H. Future changes to El Niño-Southern Oscillation temperature and precipitation teleconnections. *Geophys. Res. Lett*. **44**,10608–10616 (2017).
125. Lyon, B. The strength of El Niño and the spatial extent of tropical drought. *Geophys. Res. Lett.*, **3**, L21204 (2004).
126. Delage, F.P.D. & Power, S.B. The impact of global warming and the El Niño-Southern Oscillation on seasonal precipitation extremes in Australia. *Clim. Dyn.* **54**, 4367–4377 (2020).
127. Lin, I.-I. et al. ENSO and Tropical Cyclones. *In El Niño Southern Oscillation in a Changing Climate (eds M.J. McPhaden, A. Santoso and W. Cai). AGU Monograph*, (2020).
128. Chand, S. et al. Projected increase in El Niño-driven tropical cyclone frequency in the Pacific. *Nat. Clim. Change* **7**, 123–127 (2017).
Shows that during future climate ENSO, tropical cyclones become more frequent during El Niño and less frequent during La Niña over the off-equatorial western Pacific and central North Pacific islands.
129. Ying, J., Huang, P., Lian, T. & Chen, D. Intermodel Uncertainty in the Change of ENSO's Amplitude under Global Warming: Role of the Response of Atmospheric Circulation to SST Anomalies. *J. Clim.* **32**, 369-383 (2019).
130. Rodríguez-Fonseca, B. et al. Are Atlantic Niños enhancing Pacific ENSO events in recent decades? *Geophys. Res. Lett.* **36**, L20705 (2009).

131. Ding, H., Keenlyside, N. S., & Latif, M. Impact of the equatorial Atlantic on the El Niño Southern Oscillation. *Clim. Dyn.* **38**, 1965-1972 (2012).
132. Ham, Y.-G., Kug, J.-S., Park, J.-Y., & Jin, F.-F. Sea surface temperature in the north tropical Atlantic as a trigger for El Niño/Southern Oscillation events. *Nat. Geosci.* **6**, 112–116 (2013).
133. Kug, J.-S., & Kang, I.-S. Interactive feedback between ENSO and the Indian Ocean. *J. Clim.* **19**, 1784–1801 (2006).
134. Cai, W., Sullivan, A., & Cowan, T. Interactions of ENSO, the IOD, and the SAM in CMIP3 models. *J. Clim.* **24**, 1688-1704 (2011).
135. Kucharski, F., Syed, F. S., Burhan, A., Farah, I., & Gohar, A. Tropical Atlantic influence on Pacific variability and mean state in the twentieth century in observations and CMIP5. *Clim. Dyn*. **44**, 881–896 (2015).
136. Choi, J. Y., Ham, Y. G., & McGregor, S. Atlantic-Pacific SST Gradient Change Responsible for the Weakening of North Tropical Atlantic-ENSO Relationship due to Global Warming. *Geophys. Res. Lett.* **46**, 7574-7582 (2019).
137. Jia, F., Wu, L., Gan, B., & Cai, W. Global warming attenuates the tropical Atlantic-Pacific teleconnection. *Sci. Rep.* **6**, 20078 (2016).
138. Jia, F. et al. Weakening Atlantic Niño-Pacific connection under greenhouse warming. *Sci. Adv.* **5**, eaax4111 (2019).
139. Kug, J.-S., Vialard, J., Ham, Y.-G., Yu, J.-Y. & Lengaigne, M. ENSO Remote Forcing. *In El Niño Southern Oscillation in a Changing Climate (eds M.J. McPhaden, A. Santoso and W. Cai). AGU Monograph*, (2020)
140. Cheng, W., Chiang, J. C. H., & Zhang, D. Atlantic Meridional Overturning Circulation (AMOC) in CMIP5 Models: RCP and Historical Simulations, *J. Clim.* **26**, 7187-7197 (2013).
141. Park, J. H. et al. Effect of recent Atlantic warming in strengthening Atlantic–Pacific teleconnection on interannual timescale via enhanced connection with the Pacific meridional mode. *Clim. Dyn.* **53**, 371–387 (2019).
142. Wang, L., Yu, J.-Y. & Paek, H. Enhanced biennial variability in the Pacific due to Atlantic capacitor effect. *Nat. Commun.* **8**, 14887 (2017).
143. Le, T., & Bae, D.-H. Causal links on interannual timescale between ENSO and the IOD in CMIP5 future simulations. *Geophys. Res. Lett.* **46**, 2820–2828 (2019).
144. Sun, D.-Z., et al. Radiative and dynamical feedbacks over the equatorial cold tongue: results from nine atmospheric GCMs. *J. Clim.* **19**, 4059–4074 (2006).
145. Lloyd, J., Guilyardi, E., Weller, H. & Slingo, J. The role of atmosphere feedbacks during ENSO in the CMIP3 models. *Atmos. Sci. Lett*. **10**, 170–176 (2009).
146. Beobide-Arsuaga, G. et al. Uncertainty of ENSO-amplitude projections in CMIP5 and CMIP6 models. *Clim. Dyn.*, 1-14 (2021).
147. Guilyardi, E., Capotondi, A., Lengaigne, M., Thual, S. & Wittenberg, A. T. ENSO Modeling. *In El Niño Southern Oscillation in a Changing Climate (eds M.J. McPhaden, A. Santoso and W. Cai). AGU Monograph*, (2020)

148. Bellenger, H., Guilyardi, E., Leloup, J. Lengaigne, M., & Vialard, J. ENSO representation in climate models: From CMIP3 to CMIP5. *Clim. Dyn.* **42**, 1999–2018 (2014).
149. Kim, S.-T., Cai, W., Jin, F.-F., & Yu, J.-Y. ENSO stability in coupled climate models and its association with mean state. *Clim. Dyn.* **42**, 3313–3321 (2014).
150. Bayr, T., Wengel, C., Latif, M., Dommenget, D., Lübbecke, J., & Park, W. Error compensation of ENSO atmospheric feedbacks in climate models and its influence on simulated ENSO dynamics. *Clim. Dyn.* **53**, 155–172 (2019)
151. Watanabe, T. et al , Permanent El Niño during the Pliocene warm period not supported by coral evidence. *Nature* **471**, 209–211 (2011).
152. White, S. M., & Ravelo, A. C.. Dampened El Niño in the early Pliocene warm period. *Geophys. Res. Lett.* **47**, e2019GL085504 (2020).
153. Fedorov, A. et al. The Pliocene paradox (mechanisms for a permanent El Niño), Science 312 1485–1489 (2006).
154. Steph, S., et al. Early Pliocene increase in thermohaline overturning: A precondition for the development of the modern equatorial Pacific cold tongue, *Paleoceanography,* **25**, PA2202 (2010).
155. Manucharyan, G. E. & Fedorov, A. V. Robust ENSO across a Wide Range of Climates, *J. Clim.* **27**, 5836-5850 (2014).
156. Ford, H. L., A. C. Ravelo, & P. J. Polissar. Reduced El Niño–Southern Oscillation during the Last Glacial Maximum. *Science* **347**, 255–258 (2015).
157. Koutavas, A. & S. Joanides El Niño-Southern Oscillation extrema in the Holocene and Last Glacial Maximum, *Paleoceanography* **27**, PA4208 (2012).
158. Rustic, G. T., Koutavas, A., Marchitto, T. M. & Linsley, B. K. Dynamical excitation of the tropical Pacific Ocean and ENSO variability by Little Ice Age cooling. *Science* **350**, 1537–1541 (2015).
159. Sadekov, A., Ganeshram, R., Pichevin, L., Berdin, R., McClymont, E., Elderfield, H. & Tudhope, A. W. Palaeoclimate reconstructions reveal a strong link between El Niño–Southern Oscillation and tropical Pacific mean state. *Nat. Commun.* **4**, 2692 (2013).
160. Glaubke, R. H., Thirumalai, K., Schmidt, M. W. & Hertzberg, J. E. Discerning Changes in High□Frequency Climate Variability Using Geochemical Populations of Individual Foraminifera, *Paleoceanogr. Paleoclimatol.* **36**, (2021).
161. Wyman, D. A., Conroy, J. L., & Karamperidou, C. The Tropical Pacific ENSO–Mean State Relationship in Climate Models over the Last Millennium, *J. Clim.* **33**, 7539-7551 (2020).
162. Timmermann, A., & Jin, F. F. A nonlinear mechanism for decadal El Niño amplitude changes. *Geophys. Res. Lett.* **29**, 3-1 (2002).
163. Hayashi, M. & Jin, F. F. Subsurface nonlinear dynamical heating and ENSO asymmetry. *Geophys. Res. Lett.* **44**, 12-427 (2017).
164. Conroy, J., J. T. Overpeck, & J. E. Cole El Niño/Southern Oscillation and changes in the zonal gradient of tropical Pacific sea surface temperature over the last 1.2

ka. *PAGES News* **18**, 32–34 (2010).
165. Rustic, G. T., Polissar, P. J., Ravelo, A. C., & White, S. M. Modulation of late Pleistocene ENSO strength by the tropical Pacific thermocline, *Nat. Commun.* **11,** 5377 (2020).
166. Liu, Z. Y. et al. Evolution and forcing mechanisms of El Niño over the past 21,000 years. *Nature* **515**, 550-553 (2014).
167. Karamperidou, C., Di Nezio, P. N., Timmermann, A., Jin, F.-F. & Cobb, K. M. The response of ENSO flavors to mid-Holocene climate: Implications for proxy interpretation. *Paleoceanography* **30**, 527 (2015).
168. Chen, L., Zheng, W. & Braconnot, P. Towards understanding the suppressed ENSO activity during mid-Holocene in PMIP2 and PMIP3 simulations. *Clim. Dyn.* **53**, 1095–1110 (2019).
169. Masson-Delmotte, V. et al. Information from paleo-climate archives. *Climate Change 2013: The Physical Science Basis (eds.T. F. Stocker et al.), Cambridge University Press*, 383–464 (2013).
170. Tudhope, A. W. et al. Variability in the El Niño-Southern oscillation through a glacial-interglacial cycle, *Science* **291**, 1511–1517 (2001).
171. Emile-Geay, J. Links between tropical Pacific seasonal, interannual and orbital variability during the Holocene, *Nat. Geosci. **9***, 168-173 (2016)
172. Carré, M. et al. Holocene history of ENSO variance and asymmetry in the eastern tropical Pacific. *Science* **345**, 1045 (2014).
173. White, S. M., Ravelo, A. C. & Polissar, P. J. Dampened El Niño in the early and mid-Holocene due to insolation-forced warming/deepening of the thermocline, *Geophys. Res. Lett.* **45**, doi: 10.1002/2017GL075433 (2018).
174. Rodbell, D. T., Seltzer, G. O., Anderson, D. M., Abbott, M. B., Enfield, D. B. & Newman, J. H. An ~15,000 year record of El Niño-driven alluviation in southwestern Ecuador, *Science* **283**, 516-520 (1999).
175. Moy, C. M., G. O. Seltzer, D. T. Rodbell, & D. M. Anderson Variability of El Niño-Southern Oscillation activity at millennial timescales during the Holocene epoch, *Nature* **420,** 162-165 (2002)**.**
176. Conroy, J. L., Overpeck, J. T., Cole, J. E., Shanahan, T. M. & Steinitz-Kannan, M. Holocene changes in eastern tropical Pacific climate inferred from a Galápagos lake sediment record, *Quat. Sci. Rev.* **27,** 1166-1180 (2008).
177. Zhang, Z., Leduc, G. & Sachs, J. P. El Niño evolution during the Holocene revealed by a biomarker rain gauge in the Galápagos Islands, *Earth Planet. Sci. Lett.* **404**, 420-434 (2014).
178. Chen, S., Hoffmann, S. S., Lund, D. C., Cobb, K. M., Emile-Geay, J. & Adkins, J. F. A high-resolution speleothem record of western equatorial Pacific rainfall: Implications for Holocene ENSO evolution, *Earth Planet. Sci. Lett.* **442**, 61-71 (2016).
179. Karamperidou, C. et al. ENSO diversity and teleconnections in the Holocene: the impact of Eastern, Central and Coastal El Nino in proxy-critical locations, submitted (2021)
180. McGregor, S., Khodri, M., Maher, N., Ohba, M., Pausata, F. S. R., & Stevenson, S.

The effect of strong volcanic eruptions on ENSO. *In El Niño Southern Oscillation in a Changing Climate (eds M.J. McPhaden, A. Santoso and W. Cai). AGU Monograph*, (2020)

181. Adams, J. B., Mann, M. E. & Ammann, C. M. Proxy evidence for an El Nino-like response to volcanic forcing. *Nature* **426**, 274-278 (2003).
182. Emile-Geay, J., Seager, R., Cane, M. A., Cook, E. R., & Haug, G. H. Volcanoes and ENSO over the Past Millennium, *J. Clim.* **21**, 3134-3148 (2008).
183. Ohba, M., Shiogama, H., Yokohata, T. & Watanabe, M. Impact of strong tropical volcanic eruptions on ENSO simulated in a coupled GCM, *J. Clim.* **26**, 5169–5182 (2013).
184. Stevenson, S., Otto-Bliesner, B., Fasullo, J., & Brady, E. "El Niño like" hydroclimate responses to last millennium volcanic eruptions. *J. Clim.* ***29***, 2907-2921 (2016).
185. Khodri, M. et al., Tropical explosive volcanic eruptions can trigger El Nino by cooling tropical Africa, *Nat. Commun.* **8**, 1-13 (2017).
186. McGregor, S. & Timmermann, A. The Effect of Explosive Tropical Volcanism on ENSO. *J. Clim.* **24**, 2178-2191 (2011).
187. Zanchettin, D. et al. Bidecadal variability excited in the coupled ocean–atmosphere system by strong tropical volcanic eruptions. *Clim. Dyn.* **39**, 419–444 (2012).
188. Robock, A. Volcanic eruptions and climate, *Rev. Geophys.* **38**, 191–219 (2000).
189. Ding, Y., J. A. Carton, G. A. Chepurin, G. Stenchikov, A. Robock, L. T. Sentman, & J. P. Krasting, Ocean response to volcanic eruptions in Coupled Model Intercomparison Project 5 (CMIP5) simulations, *J. Geophys. Res. Oceans.* **119**, 5622–5637 (2014).
190. Dee, S. G. et al. No consistent ENSO response to volcanic forcing over the last millennium. *Science* **367**, 1477–1481 (2020).
Shows that proxy records reveal an insignificant tendency for an El Nino-like response in the year after a strong volcanic eruption, at odds with the strong tendencies found in climate models.
191. Pausata, F. S. R., Karamperidou, C., Caballero, R., & Battisti, D. S. ENSO response to high-latitude volcanic eruptions in the northern hemisphere: The role of the initial conditions. *Geophys. Res. Lett.* **43**, 8694-8702 (2016).
192. Stevenson, S., Fasullo, J. T., Otto-Bliesner, B. L., Tomas, R. A., & Gao, C. Role of eruption season in reconciling model and proxy responses to tropical volcanism. *Proc. Natl. Acad. Sci.* **114**, 1822–1826 (2017).
193. Zanchettin, D. et al. Clarifying the relative role of forcing uncertainties and initial-condition unknowns in spreading the climate response to volcanic eruptions. *Geophys. Res. Lett.* **46**, 1602–1611 (2019).
194. Pausata, F. S. R., Zanchettin, D., Karamperidou, C., Caballero, R., & Battisti,D. S. ITCZ shift and extratropical teleconnections drive enso response to volcanic eruptions. *Sci. Adv.* **6**, eaaz5006 (2020)
195. Predybaylo, E. et al. El Niño/Southern Oscillation response to low-latitude volcanic eruptions depends on ocean pre-conditions and eruption timing. *Commun Earth Environ* **1**, 1-13 (2020)

196. Emile-Geay, J., & Tingley, M. Inferring climate variability from nonlinear proxies: application to palaeo-enso studies. *Clim. Past* **12**, 31–50 (2016).
Demonstrates the pitfalls of ignoring nonlinearities in the proxy–climate relationship, which often exaggerates climate variability changes inferred by proxies and leads to reconstructions with poorly quantified uncertainties.
197. Kiefer, J., & Karamperidou, C. High-resolution modeling of enso-induced precipitation in the tropical andes: Implications for proxy interpretation. *Paleoceanogr. Paleoclimatol.* **34**, 217-236 (2019).
198. Dee, S., Okumura, Y., Stevenson, S., & Di Nezio, P. Enhanced North American ENSO Teleconnections During the Little Ice Age Revealed by Paleoclimate Data Assimilation. *Geophys. Res. Lett.* **47**, e2020GL087504 (2020).
199. Chang, P. et al. Pacific meridional mode and El Niño-Southern Oscillation. *Geophys. Res. Lett.* **34**, L16608 (2007).
200. Vimont, D. J., Alexander, M. & Fontaine, A. Midlatitude excitation of tropical variability in the Pacific: The role of thermodynamic coupling and seasonality. *J. Clim.* **22**, 518-534 (2009).
201. Stuecker, M. F. Revisiting the Pacific Meridional Mode, *Sci. Rep.* **8**, 1-9 (2018).
202. Hong, L. C., & Jin, F. F. A southern hemisphere booster of super El Niño. *Geophys. Res. Lett.* **41**, 2142-2149 (2014).
203. Holmes, R. M., McGregor, S., Santoso, A. & England, M. H. Contribution of Tropical Instability Waves to ENSO Irregularity. *Clim. Dyn.* **52**, 1837-1855 (2019).
204. Bony, S. & Dufresne, J. L. Marine boundary layer clouds at the heart of tropical cloud feedback uncertainties in climate models. *Geophys. Res. Lett.* **32,** L20806 (2005).
205. Deser, C. et al. Insights from Earth system model initial-condition large ensembles and future prospects. *Nat. Clim. Change* **10**, 277–286 (2020)
206. Hawkins, E. & Sutton, R. Time of emergence of climate signals. *Geophys. Res. Lett.* **39,** L01702 (2012).
207. Jochum, M. & Murtugudde, R. Temperature advection by tropical instability waves. *J. Phys. Oceanogr.* **36**, 592-605 (2006).
208. An, S. I. Interannual Variations of the Tropical Ocean Instability Wave and ENSO. *J. Clim.* **21**, 3680-3686 (2008).
209. Chu, J.-E. et al. Reduced tropical cyclone densities and ocean effects due to anthropogenic greenhouse warming. *Sci. Adv.* **6**, eabd5109 (2020).
210. Bartlein, P. J. & Shafer, S. L. Paleo calendar-effect adjustments in time-slice and transient climate-model simulations (PaleoCalAdjust v1.0): impact and strategies for data analysis, *Geosci. Model Dev.* **12**, 3889–3913 (2019).

Acknowledgements

This work is supported by the Strategic Priority Research Program of Chinese Academy of Sciences, Grant No. XDB40000000. W.C., A.S., B.N., and G.W. are supported by Centre for Southern Hemisphere Oceans Research (CSHOR) a joint research facility between QNLM

and CSIRO (CSHOR). We acknowledge the World Climate Research Programme, which, through its Working Group on Coupled Modelling, coordinated and promoted CMIP6. We thank the climate modelling groups for producing and making available their model output, the Earth System Grid Federation (ESGF) for archiving the data and providing access, and the multiple funding agencies who support CMIP6 and ESGF. PMIP is endorsed by both WCRP/WGCM and Future Earth/PAGES. MFS was supported by NOAA's Climate Program Office's Modeling, Analysis, Predictions, and Projections (MAPP) program grant NA20OAR4310445 and participates in the MAPP Marine Ecosystem Task Force. This is PMEL contribution number 5213. M.L. is supported by the ARISE ANR (Agence Nationale pour la Recherche) project (ANR□18□CE01□0012). Xiaopei L. is supported by the National Natural Science Foundation of China (41925025 and 92058203). B.G. was supported by the National Natural Science Foundation of China (41922039). A.C. is supported by the NOAA Climate Program Office Climate Variability and Predictability (CVP), and Modeling, Analysis, Predictions and Projections (MAPP) Programs. M.C. was supported by NERC grant NE/S004645/1. This is IPRC publication 1525 and SOEST contribution 11356. A.S.T. is supported by the Australian Research Council (ARC FT160100495). S.-W.Y. is funded by the Korean Meteorological Administration Research and Development Program under grant (KMI2020-01213). Y.Y. is supported by the National Natural Science Foundation of China (NSFC) project (grant no. 41976005). Xichen L. is supported by National Key R&D Program of China (2018YFA0605703) and the National Natural Science Foundation of China (Grants 41976193). M.C. is supported by NERC grant NE/S004645/1. T.B. is funded by Deutsche Forschungs Gemeinschaft (DFG) project "Influence of Model Bias on ENSO Projections of the 21st Century" through grant 429334714. C.K. is supported by US NSF Award AGS-1902970. J.R.B. acknowledges support from the ARC Centre of Excellence for Climate Extremes (CE170100023). J.Y. is supported by National Natural Science Foundation of China (Grants 41690121, 41690120). A.T. was supported by the Institute for Basic Science (IBS-R028-D1). S.M. acknowledges support from the Australian Research Council through grant number Ft160100162. J.-S.K. is supported by the National Research Foundation of Korea (NRF-2018R1A5A1024958). X.-T. Z. is funded by the National Natural Science Foundation of China (41975092). B.D. acknowledges support from Fondecyt (Grant 1190276) and ANR (Grant ANR-18-CE01-0012).

Author contributions

W.C. and A.S. conceived the study. W.C., M.J.M., M.F.S., M.L., A.S., J-S.K., A.S.T., S.-W. Y., C.K., B.D., M.C., A.T. coordinated the presentation and discussion for various sections. F.J., B.N., G.W., Y.Y., J.Y. contributed to analysis and graphic of various figures. All authors contributed to the manuscript preparation, interpretation, discussion, and writing, led by W.C.

Competing interests

The authors declare no competing interests.